# THEMATIC SECTION: 7TH WORLD CONGRESS ON INTEGRATED COMPUTATIONAL MATERIALS ENGINEERING



# Lifetime and Degradation Study of Poly(Methyl Methacrylate) via a Data-Driven Study Protocol Approach

Hein Htet Aung<sup>1,2</sup> • Donghui Li<sup>1,3</sup> • Jiqi Liu<sup>1</sup> • Chiara Barretta<sup>4</sup> • Yiyang Sheng<sup>5</sup> • Yea Jin Jo<sup>1</sup> • Jayvic C. Jimenez<sup>6,7</sup> • Erika I. Barcelos<sup>1,7</sup> • Gernot Oreski<sup>4</sup> • Roger H. French<sup>1,7,8,9</sup> • Laura S. Bruckman<sup>1,2</sup>

Received: 1 September 2023 / Accepted: 27 October 2023 / Published online: 22 November 2023 © The Minerals, Metals & Materials Society 2023

#### **Abstract**

To optimize and extend the service life of polymeric materials in outdoor environments, a domain knowledge-based and data-driven approach was utilized to quantitatively investigate the temporal evolution of degradation modes, mechanisms, and rates under various stepwise accelerated exposure conditions. Six formulations of poly(methyl methacrylate) (PMMA) with different combinations of stabilizing additives, including one unstabilized formulation, were exposed in three accelerated weathering conditions. Degradation was dependent on wavelength as samples in UV light at 340 nm (UVA) exposure showed the most yellowing. The unstabilized PMMA formulation showed much higher yellowness index values (59.5) than stabilized PMMA formulations (2–12). Urbach edge analysis shows a shift toward longer wavelength from 285 to 500 nm with increasing exposure time and an increased absorbance around 400 nm of visible region as the unstabilized samples increase in yellowing. The degradation mechanisms of PMMA were tracked using induced absorbance to dose at specific wavelengths that correspond to known degradation mechanisms. The degradation pathway of PMMA was modeled in a *Stressor | Mechanism | Response>* framework using network structural equation modeling (netSEM). netSEM showed changes in degradation pathway as PMMA transition stages of degradation.

 $\textbf{Keywords} \ \ Polymer \ degradation \cdot PMMA \cdot UV \ absorber \cdot HALS \cdot Antioxidant \cdot Optical \ properties \cdot netSEM \cdot Degradation \ pathway \ models$ 

# Introduction

Polymers are ubiquitous and have been long-standing materials given that they are cheap, easily manufactured, versatile, and most importantly, durable [1–5]. Despite all the benefits, polymers will invariably undergo degradation due to environmental or other factors directly influenced by their applications. Degradation can be described as an alteration in the physical, chemical, and/or mechanical properties of a material.

Polymer degradation can manifest from environmental stressors such as heat, electromagnetic radiation, and humidity, and from various external stressors such as chemical or mechanical factors throughout its application [6]. Exposure to sunlight, for example, leads to photooxidation of the

Hein Htet Aung and Donghui Li contributed equally to this work.

Extended author information available on the last page of the article

polymer, caused by free radicals leading to chemical changes such as chain scission, changes in the polymer's functional groups, and/or cross-linking; all of these effects can alter the polymer's intrinsic properties.

Poly(methyl methacrylate) (PMMA) was first discovered during the early 1930s. Shortly after its discovery, PMMA was found to be a promising material as a substitute for inorganic glass [7]. It is widely used nowadays due to its excellent optical properties, desirable mechanical properties, and weatherability [8–21]. Despite its versatility, however, PMMA can quickly degrade in outdoor exposures due to solar irradiation, temperature, and moisture. These factors shorten the duration and lifespan of PMMA.

Photodegradation of PMMA can be inhibited and its lifetime prolonged using chemical stabilizers such as ultraviolet (UV) absorbers [22–24], hindered amine light stabilizers (HALS) [25, 26], and antioxidants [27, 28]. These stabilizers act as sacrificial agents which are preferentially photooxidized, keeping the polymer chains chemically intact. They



are often added in small quantities relative to the polymer weight, since these stabilizers act like plasticizers. They are typically incorporated within the polymer matrix during melt processing [29]. A popular example of such a class of chemical stabilizers is Tinuvin (BASF) [23]. While the incorporation of chemical preservatives helped prolong the usage of PMMA, the polymer will invariably undergo degradation at some point.

Because of PMMA's wide usage, understanding how it degrades is necessary. Fundamental studies have led to improvements such as increased durability, and literature shows progress in estimating the lifetime of PMMA [4, 5, 30–36]. Although standardized durability tests with accelerated exposures are widely used to assess failure and durability of PMMA, the results obtained are solely based on the typical pass/fail criteria, which are insufficient to describe critical features such as failure modes, degradation mechanisms, and kinetics. A reliable study protocol for evaluating degradation and predicting the lifetime is established by French et al. [37], which highlights understanding the failure modes and the degradation mechanisms responsible for the corresponding failure modes.

In this study, a similar approach was performed to investigate the degradation mechanisms from weathering of PMMA. We developed a stepwise study protocol such that we can observe the synergistic effect of stressors, which are rarely investigated. Different formulations of commercial PMMA films were exposed in three different accelerated exposure conditions according to ASTM standards [38, 39]. Chemical and mechanical properties of the samples were

characterized at each exposure step using non-destructive techniques including colorimetry, UV–Vis-NIR spectroscopy, FTIR, optical profilometry, and microindentation.

Characterization results were subsequently analyzed using a data-driven modeling technique called network structural equation modeling (netSEM). netSEM allows for exploration of variable relationships using pathway diagrams in a stressor, mechanism, and response ( $\langle S | M | R \rangle$ ) framework by describing these relationships from standard models, such as linear, quadratic, and other nonlinear forms of equations [40]. The quantified relationships describe degradation pathways which can be traced back to the exposure or weathering conditions that was captured during the lifetime studies [41–45]. The data-driven findings guided by domain knowledge rationalize the underlying mechanisms responsible for the PMMA degradation.

# **Materials and Methods**

# **Poly (Methyl Methacrylate) Formulations**

Six formulations of PMMA were investigated as summarized in Table 1. All the six formulations are optically clear and have a thickness of approximately 3 mm.

# **Accelerated Indoor Exposures**

Samples were exposed to three different types of indoor accelerated conditions according to ASTM G154 and G155

**Table 1** Summary of six PMMA formulation

Brand	PMMA formulation	Description
Brand A	UVT	UV transparent. Unstabilized PMMA formulation.
	FF1	Multi-purpose. Used in security and transport industries as substrate.
	UVA	UV absorbing. Used in applications requiring extra UV protection.
Brand B	UVO	Used for general purpose.
	UVP	Used for general purpose.
	UVF	UV filtering. Used in applications requiring extra UV protection.

Table 2 Exposure conditions of three accelerated indoor exposures based on ASTM G154 and ASTM G155 standards

Stressor	Exposure	Condition
UV, heat, humidity	Cyclic QUV	Cyclic exposure of 8 h of UVA light at 1.55 W/m <sup>2</sup> at 340 nm, 70 °C and 4 h of condensing humidity at 50 °C in dark
UV, heat	Hot QUV	Constant exposure of UVA light at 1.55 W/m $^2$ at 340 nm, 70 $^{\circ}$ C
Full spectrum light	QSUN	Cyclic exposure of 102 min of TUV light at 70 W/m <sup>2</sup> , 63 °C and 18 min of TUV light at 70 W/m <sup>2</sup> , 63 °C with water spray



standards shown in Table 2. For UV light exposures, the QUV Accelerated Weathering Tester with fluorescent UVA-340 lamps was used to simulate the effect of critical short wavelength region from normal solar cutoff at 295–365 nm, peaking at 340 nm [46]. Due to the absence of the condensing humidity cycle, the samples in Hot QUV (modified-ASTM G154 Cycle 4) has an accumulated UV dosage of 1.5 times higher than those in Cyclic QUV (ASTM G154 Cycle 4). For full spectrum light exposures, Q-SUN Xe-1/Spray was used.

Stepwise exposures of twenty-four replicate samples from each of the six formulations were assigned to three different exposure types (eight samples per formulation per exposure type) so as to provide sufficient data and observations for statistical analysis. The samples were exposed for a total of 22500 h and measured at time steps of 0 (referred to as "baseline"), 400, 800, 1200, 2200, 3200, 16200, 17400, and 22500 h. One sample was retained at each exposure step in order to preserve the stepwise information. The samples are retained for further characterization in future work.

To accurately compare the xenon arc and UV light exposures, the photodose of light between 280 and 360 nm was calculated as shown in Eq. 1 where UVA<sub>360</sub> is the integrated irradiance (J/m<sup>2</sup>) between 280 and 360 nm,  $E_{\lambda}$  is the irradiance (W/m<sup>2</sup>),  $\lambda$  is the wavelength and t is the time under exposure [47].

$$UVA_{360} = \int_0^t \int_{280}^{360} E_{\lambda} d\lambda dt$$
 (1)

The spectral characteristics of all three exposure conditions are shown in Table 3.

#### **Characterization Methods**

#### Yellowness Index (YI) and Haze

Yellowing of polymers is an indicator of polymer degradation. Yellowness Index (yi) is a quantifiable measurement of such behavior, in accordance with ASTM E313 [48]. Haze

Table 3 Spectral irradiance and accumulated photodosage at end of exposure for full spectrum, TUV, and UVA<sub>360</sub>

Calculation	Spectrum	Cyclic QUV	Hot QUV	QSUN
Irradiance	Full spectrum	56.36	84.54	390.71
$(W/m^2)$	TUV	56.36	84.54	70.00
	UVA	40.43	60.65	26.06
Exposure time (h)	-	22500	22500	22500
Photodose (MJ/m <sup>2</sup> )	UVA	3275.31	4912.96	2110.99

is the ratio of diffuse transmittance to total transmittance of incident light in the wavelength range between 380 and 780 nm measured according to ASTM D1003 [49]. Herein, colorimetric measurements were performed on an UltrascanPro spectrophotometer (HunterLab, USA) to obtain the YI and haze of the exposed samples using a D65 illuminant with viewing degree angle at 10 degrees (coefficients:  $C_x = 1.3013$ ,  $C_z = 1.1498$ ). The high-performance colorimeter allows fast and non-destructive measurements with a spectral range from 350 to 1050 nm with 5 nm interval data output. To simulate D65 daylight, a UV attenuation filter was inserted partially in the light path of spectrophotometer. A D65 light source ensures a single standard for lighting that is applied across different products, manufacturers, and industries.

# Gas Chromatography-Mass Spectrometry (GC-MS)

To determine the additives and stabilizers present in the PMMA samples, gas chromatography-mass spectrometry (GC-MS) was performed with a QM2010 Plus from Shimadzu with Pyrolyzer-3030D from Frontier Laboratories Ltd. The PMMA samples were heated in the pyrolyzer from 60 to 320 °C at a heating rate of 20 °C/min under a helium flow. The evolved gases were continuously introduced into GC-MS for identification of the substances.

#### UV-Vis-NIR

The transmittance and reflectance of the PMMA samples were measured using F10-RT (PARTS-UV) reflectometer manufactured by Filmetrics. The film coating recipe was setup as air for Medium, HC-standard-2, and Acrylic-2 for substrate.

#### Fourier Transform Infrared Spectroscopy

The infrared spectra were obtained using attenuated total reflectance fourier transform infrared spectroscopy (ATR-FTIR) with Agilent Cary 630 FTIR. Measurements were taken at a resolution of 2 cm<sup>-1</sup> with 32 background scans. The obtained spectra had no baseline correction or other post-processing performed except for peak normalization with the carbonyl peak, which found to be around 1720 cm<sup>-1</sup>.

### Microindentation

The mechanical properties of PMMA samples were investigated with microindentation test using Nanovea PB1000. Micro-Vickers test was performed on all PMMA samples with a V2830 indenter using different recipes for baseline and cracked samples. For baseline samples, a 5 N load with 10 N/min loading-unloading rate was applied with



an approach speed of  $30 \, \mu m$ . The contact load was defined at  $20 \, mN$ , and creep was applied for  $10 \, s$  with standard proportional-integral-derivative (PID) settings and Poisson's ratio set to 0.36. Five measurements at different locations on the exposed side of the samples were taken. Cracked samples were measured with the same setting as baseline samples with a reduced load of  $2 \, N$  in order to avoid introducing additional cracks from microindentation measurements. Eight measurements were taken on the exposed side for cracked samples: four measurements near the cracked regions and four measurements at non-cracked regions. The Young's modulus and Vickers hardness values were calculated using Nanovea Mech software.

#### **Surface Roughness**

Surface roughness was measured using a Zygo NewView 7300 optical profilometer. Images were captured with a 10 x magnification, 3 % threshold for min mod %, image resolution of 640 x 480 at 210 Hz, a scan length of 65  $\mu$ m and frequency domain analysis (FDA) resolution setting was set to high 2 G.

# **Data-Driven Modeling**

#### **Induced Absorbance to Dose**

In order to quantify degradation mechanisms and rates, IAD was calculated as a tracking metric. IAD measures the change in optical absorbance per centimeter of a sample per unit dosage [50, 51]. Average IAD allows tracking of phenomenon over large doses and is calculated as follows:

$$IAD = \frac{Abs_i(\lambda)/cm - Abs_0(\lambda)/cm}{Dose_i - Dose_0}$$
 (2)

where,  $Dose_0$  is the dose at baseline,  $Dose_i$  is the dose at time point i,  $Abs_0(\lambda)/cm$  is the absorbance at baseline, and  $Abs_i(\lambda)/cm$  is the absorbance at time point i. IAD is independent of thickness and is normalized over photo dosage [50], which allows comparison across samples as well as different exposure steps.

### **Urbach Parameters**

Urbach parameters were obtained to evaluate the electronic structure and bonding changes in material to describe the degree of energy disorder in the polymers [52, 53]. Onsets obtained from the UV absorption spectra were fitted. The equations shown below were then used to determine the Urbach parameters based on the fitted curves,

$$A(E) = H_A \exp(\frac{E - E_{0A}}{W_A}) \tag{3}$$



$$\ln(A) = \frac{E - (E_{0A} - h_A W_A)}{W_A},\tag{4}$$

where  $H_A$  and  $h_A$  are fitted parameters, and the relationship between absorbance, A, and frequency in eV, E, is characterized by the Urbach Width  $(W_A)$  and the Urbach edge energy  $(E_{0A})$  [54, 55].

#### Modeling in *<Stressor* | *Mechanism* | *Response>* Framework

An inferential model was built with netSEM using a Markovian (pairwise) process [40, 45, 56] to explore relationships between variable pairs. The  $\langle S \mid M \mid R \rangle$  notation in netSEM is adapted from Dirac notation (Braket notation) in quantum mechanics [57]. The adaptation in netSEM represents the pathway to *Response* (observation) due to a *Mechanism* (operator) resulting from a *Stressor* (operation). The strength of the relationship between variables was evaluated using adjusted  $R^2$  and the best relationship was selected. Model equations as well as an interpretable visual pathway diagram showing the relationship between variables were also generated. PMMA degradation was explored with UV dosage as a stressor, IAD metrics as mechanistic variables to track degradation mechanisms, and yellowness index as a response.

# Results

# Detection of Additives in PMMA by GC-MS and UV-Vis

The types of additives in baseline samples of the six formulations of PMMA were determined using pyrolysis GC-MS. The samples mainly contained three types of UV stabilizers: antioxidant, hindered amine light stabilizer (HALS), and UV light absorbers. The specific chemical compounds corresponding to the formulation of PMMA are shown in Table 4, and the chemical structures of the compounds are shown in Fig. 1.

Tinuvin 292 (HALS), as shown in Fig. 1, is a combination of two compounds that are developed especially for coatings. Tinuvin P and Tinuvin 327, belong to a class of UV absorbers called phenolic benzotriazoles which features strong absorption between 300 and 400 nm with minimal absorbance in the visible range (>400 nm) providing UV protection for PMMA. Lastly, antioxidant Irganox 1076 is a non-discoloring stabilizer that protects polymers against thermo-oxidative degradation.

The presence of additives in PMMA formulations can also be inferred from comparing the UV–Vis spectrum of baseline unstabilized UVT formulation to the remaining formulations, as shown in Fig. 2. Peaks at 298 nm and 330 nm

Table 4 Information on additives detected in baseline PMMA samples determined by GC-MS

PMMA formulation	Brand	Antioxidant	HALS	UV absorber
UVT	A	_	_	_
FF1	A	_	_	Tinuvin P (possible fragment)
UVA	A	Irganox 1076	Tinvin 292	_
UVO	В	Irganox 1076	_	_
UVP	В	Irganox 1076	_	Tinuvin P, Tinuvin 327
UVF	В	Irganox 1076	-	Tinuvin P, Tinuvin 327

<sup>&#</sup>x27;-' indicates that the stabilizer was undetected

Fig. 1 Chemical structures of additives in PMMA formulations identified by GC-MS. Top Left: Tinuvin 292 (HALS), Top Right: Tinuvin P (UV absorber), Bottom Left: Irganox 1076 (Antioxidant), Bottom Right: Tinuvin 327 (UV absorber)

can be observed for FF1 formulation, indicating the presence of Tinuvin P. UVP and UVF, which have the same additives, as identified by GC-MS, also show the same UV-Vis spectrum. The smaller width peak around 350 nm in UVO compared to that of UVP and UVF hints the abscence of some additives that are found in UVP and UVF. The UV-Vis

Antioxidant: Irganox 1076

spectrum for UVA shows the broadest range compared to the rest of the PMMA formulation.

# **PMMA Samples Throughout Exposure**

The degradation of PMMA samples were visually observable through the exposure steps, especially for unstabilized



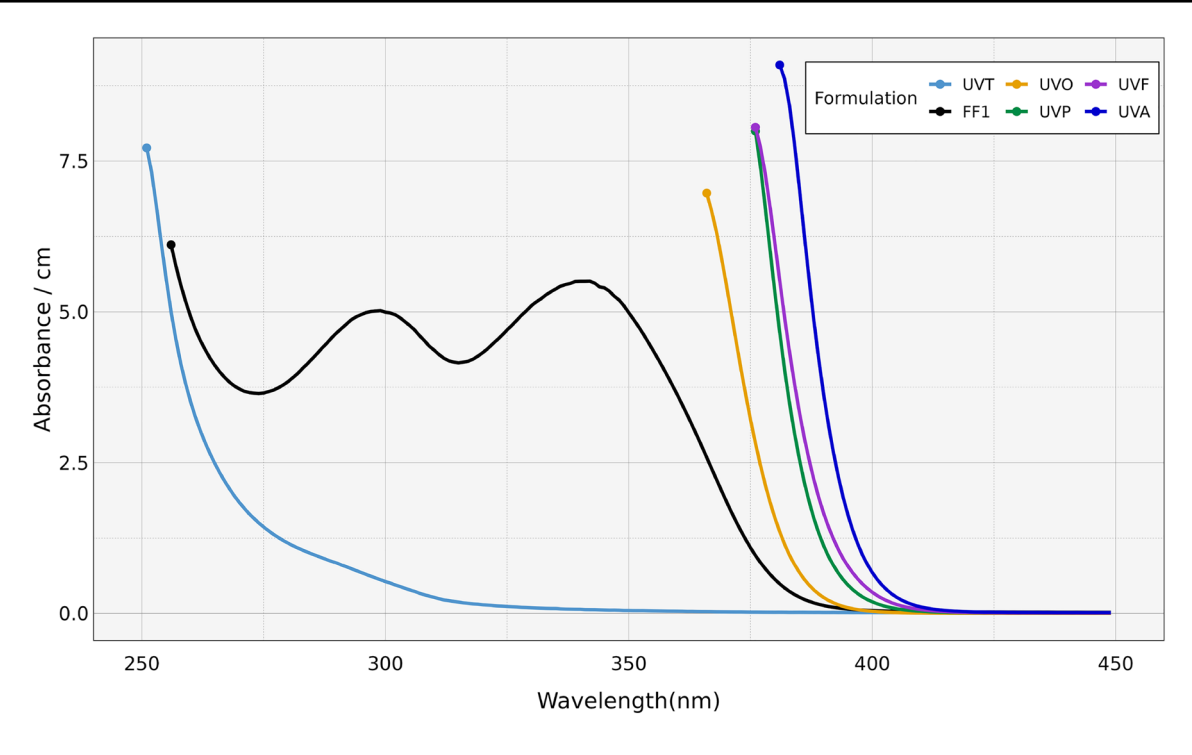
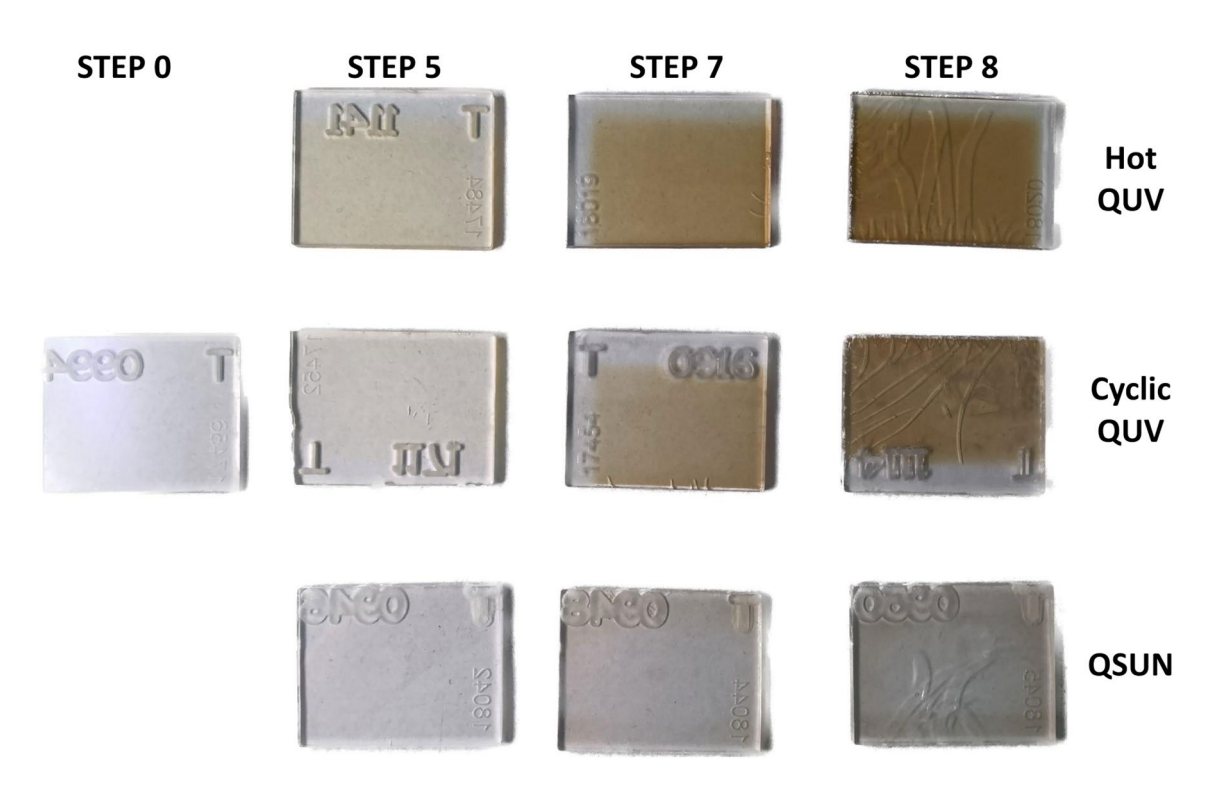


Fig. 2 The UV-Vis absorbance per cm spectrum of baseline samples for six formulations of PMMA. UVT is the unstabilized formulation. Spectrum to the left of the points is excluded due to saturation



**Fig. 3** Changes in UVT samples at exposure steps 0, 5 (3200 h), 7 (17400 h), and 8 (22500 h) for exposure conditions Hot QUV, Cyclic QUV, and QSUN. Hot QUV contains stressors UV and Tempera-

ture. Cyclic QUV contains stressors UV, Temperature, and Humidity. QSUN contains stressors Full Spectrum Light and Humidity



UVT samples. Figure 3 shows the changes in UVT samples at exposure steps 0, 5, 7, and 8 across the different exposure conditions. The gradual increase in yellowing of the samples can be observed from step 0 to step 8 for Hot QUV and Cyclic QUV exposure conditions. At step 8, cracks can be observed on samples across all exposure conditions.

#### Yellowness Index and Haze

The YI value was measured to assess the degree of yellowing and therefore the extent of degradation in PMMA samples under exposure. Figure 4 shows a multi-panel plot of yellowness index of PMMA with the faceting groups on the rows as three exposure conditions and the columns as six PMMA formulations.

Among the six formulations, the UVT samples show the highest YI values in all exposure conditions, followed by FF1 samples, compared to other PMMA formulations. Comparing across exposure conditions, samples in Hot QUV (HQUV) exposure have the highest YI values.

In addition to discoloration, PMMA degradation can also occur as loss in optical clarity, which is quantified by haze (%). Figure 5 shows the haze (%) values as a multi-panel plot with facet columns as PMMA formulations and facet rows as exposure conditions. Although there is no clear trend in haze

(%) values across different PMMA formulations, samples in QSUN show significantly higher haze (%) values compared to samples in other exposure conditions.

#### Induced Absorbance to Dose (IAD)

The degradation mechanisms and their rates for PMMA photodegradation were evaluated with changes in IAD metrics calculated from the absorbance/cm spectrum from UV–Vis measurements. The positive IAD values indicate a photodarkening process while negative IAD values indicate a photobleaching process. Figure 6 shows a multi-panel plot with exposure conditions as columns and the formulations UVT and FF1, which were formulations that showed highest yi values, as rows. IAD was tracked at specific wavelengths that correspond to known degradation mechanisms in PMMA:

- IAD at 275 nm (IAD<sub>275</sub>): Changes in fundamental absorption edge of PMMA.
- IAD at 298 and 339 nm (IAD<sub>298</sub>, IAD<sub>339</sub>): Photobleaching of Tinuvin P.
- IAD at 400 nm (IAD<sub>400</sub>): Formation of chromophores responsible for yellowing.

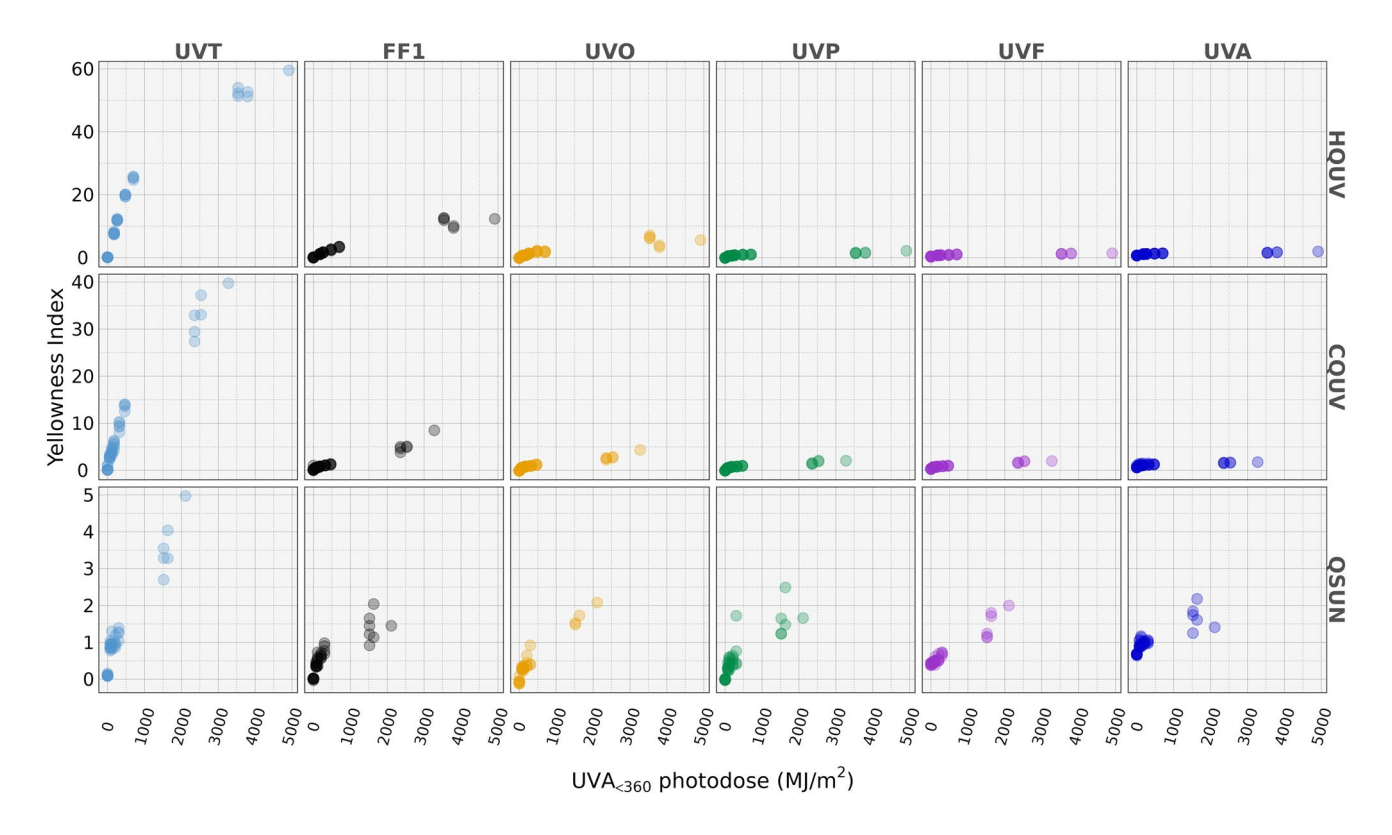


Fig. 4 Yellowness index (YI) plotted against photodosage of UVA $_{<360}$  for the six formulations of PMMA under Hot QUV (HQUV), Cyclic QUV (CQUV), and QSUN exposure. Note the scale for yi is different for each exposure condition



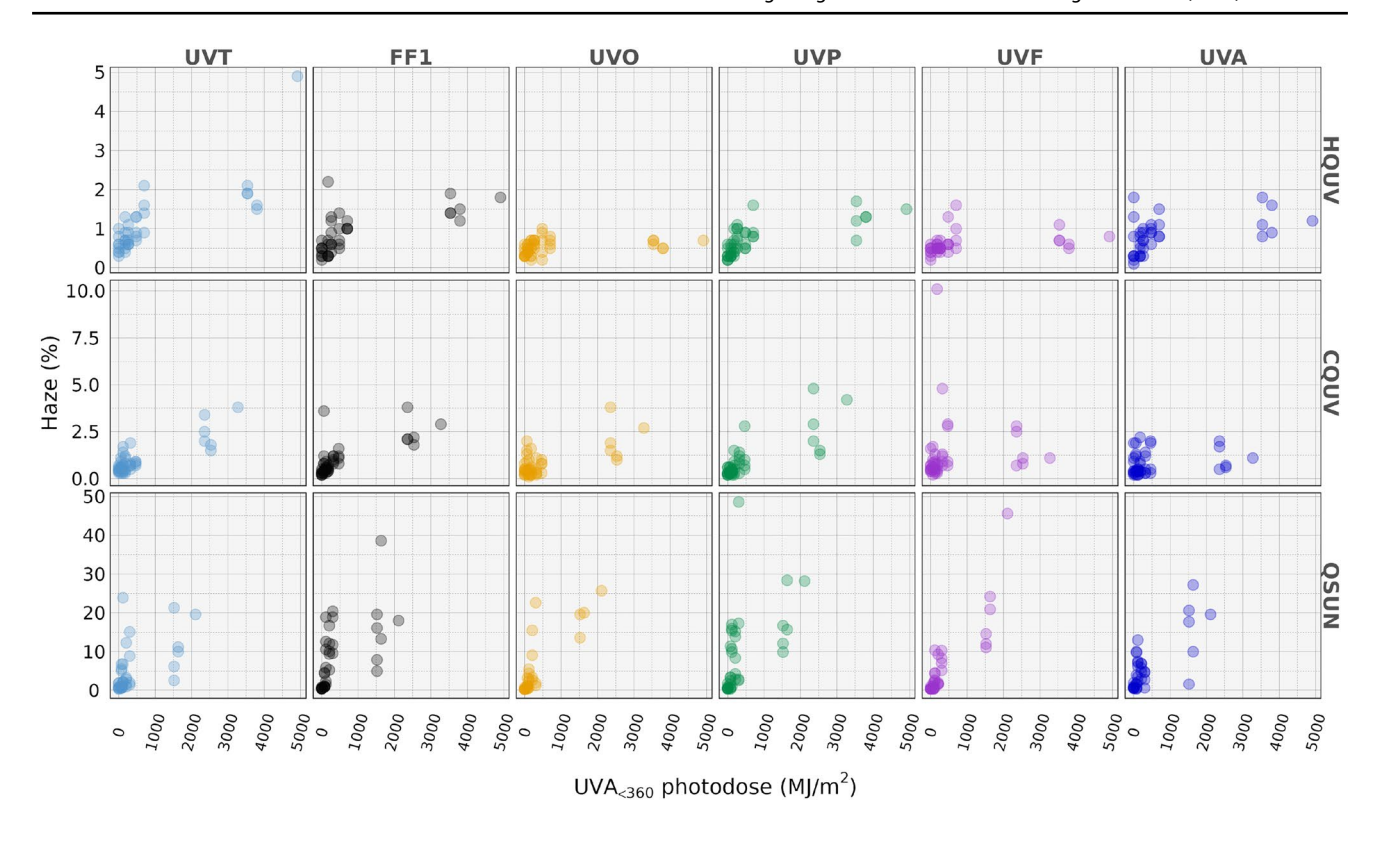


Fig. 5 Haze (%) plotted against photodosage of UVA $_{<360}$  for the six formulations of PMMA under Hot QUV (HQUV), Cyclic QUV (CQUV) and QSUN exposure. Note the scale for haze (%) is different for each exposure condition

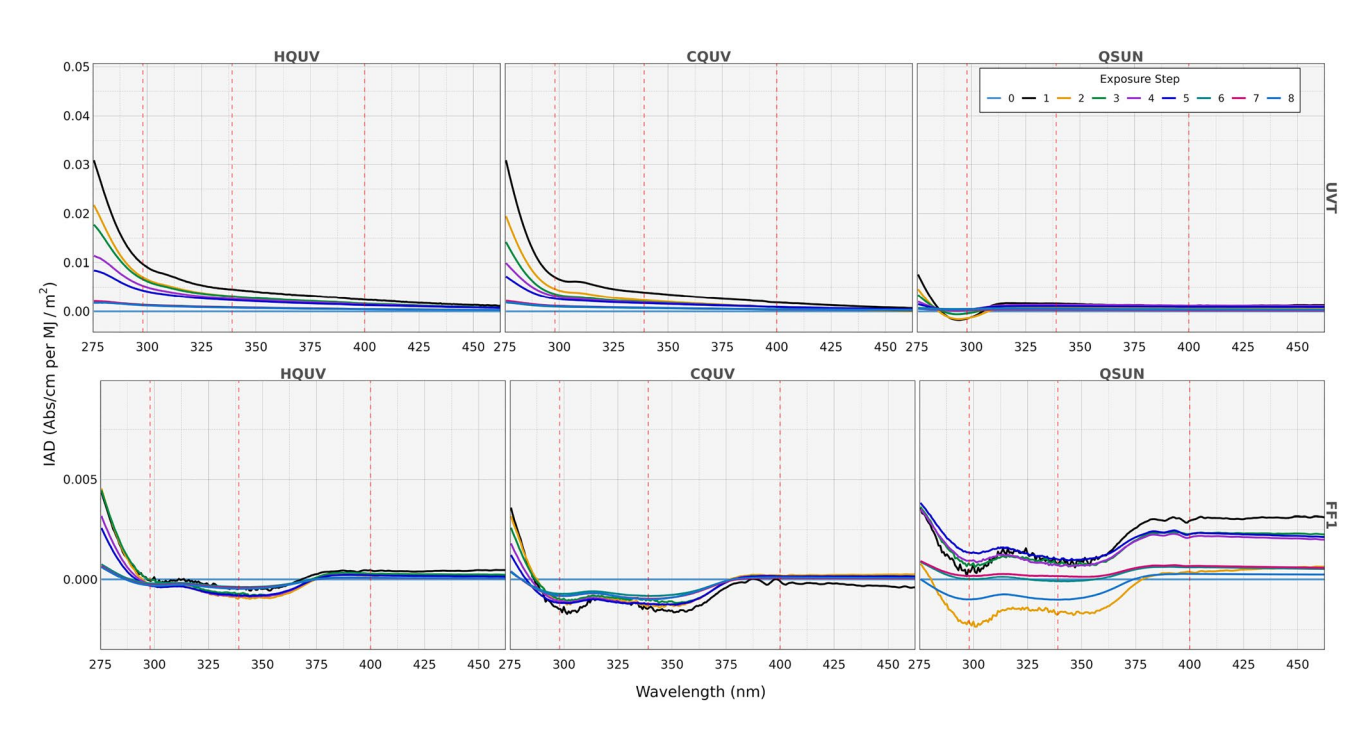


Fig. 6 Induced absorbance to dose value for unstabilized UVT and stabilized FF1 under exposure conditions Hot QUV (HQUV), Cyclic QUV (CQUV), and QSUN. Vertical dashed lines indicate wavelengths at 298, 339, and 400 nm

The IAD spectrum follows a consistent trend for HQUV and CQUV exposures for both UVT and FF1 formulation

throughout the exposure steps. Additionally for FF1 samples, a photobleaching effect can be observed at 298 nm and 339



nm, depicted by negative IAD values. For QSUN exposure, UVT shows a photobleaching process around 300 nm, which was not observed in other exposure conditions. FF1 formulation did not have a clear trend for IAD spectrum throughout the exposure step. UVT also shows higher IAD values than FF1 formulation by approximately one magnitude.

# **Urbach Edge Fitting**

Urbach edge fitting from the absorption spectra for all PMMA formulations prior to exposure is shown in Fig. 7. The onset of UVT occurs below 300 nm, while the other samples have onsets occurring above 375 nm.

Urbach edge fitting to the absorption spectra was also performed on PMMA samples from steps 0–8. We focus our attention specifically at UVT and FF1, which are shown in Figs. 8 and 9, respectively, because there are no significant changes from the Urbach edge positions and width with the remaining PMMA formulations.

The Urbach edge positions and widths for all six PMMA formulations prior to exposure are summarized in Table 5. Formulations with additives have Urbach edges at longer wavelengths. Due to the different chemistry of the UV absorbers, the Urbach edge width varies with different

formulations. UVT, which has no UV absorbers, has an Urbach edge at 285 nm.

Tables 6 and 7 summarize the results for Urbach edge position and width for UVT and FF1 formulations in exposure, respectively. Compared to the significant shift in Urbach edge position from 285–500 nm for UVT formulation, the Urbach edge position for FF1 formulation remains around 376–378 nm.

# <Stressor | Mechanism | Response> Models

After quantifying performance and exposure metrics as well as degradation mechanisms, data-driven modeling in a  $\langle Stressor \mid Mechanism \mid Response \rangle$  ( $\langle S \mid M \mid R \rangle$ ) framework using the netSEM-markovian model was performed to understand and explore the degradation pathways of PMMA. In the context of the  $\langle S \mid M \mid R \rangle$  framework, UV dosage was defined as a stressor, IAD values as mechanistic variables, and YI as response.

The degradation of PMMA was modeled in three different phases corresponding to the changes observed at exposure steps 5, 7, and 8. netSEM-markovian models the relationship between each variable pair with linear and nonlinear forms of equations and returns the best fit equation by determining the highest adjusted  $R^2$ . The results for unstabilized UVT and stabilized FF1 samples in Hot QUV samples are

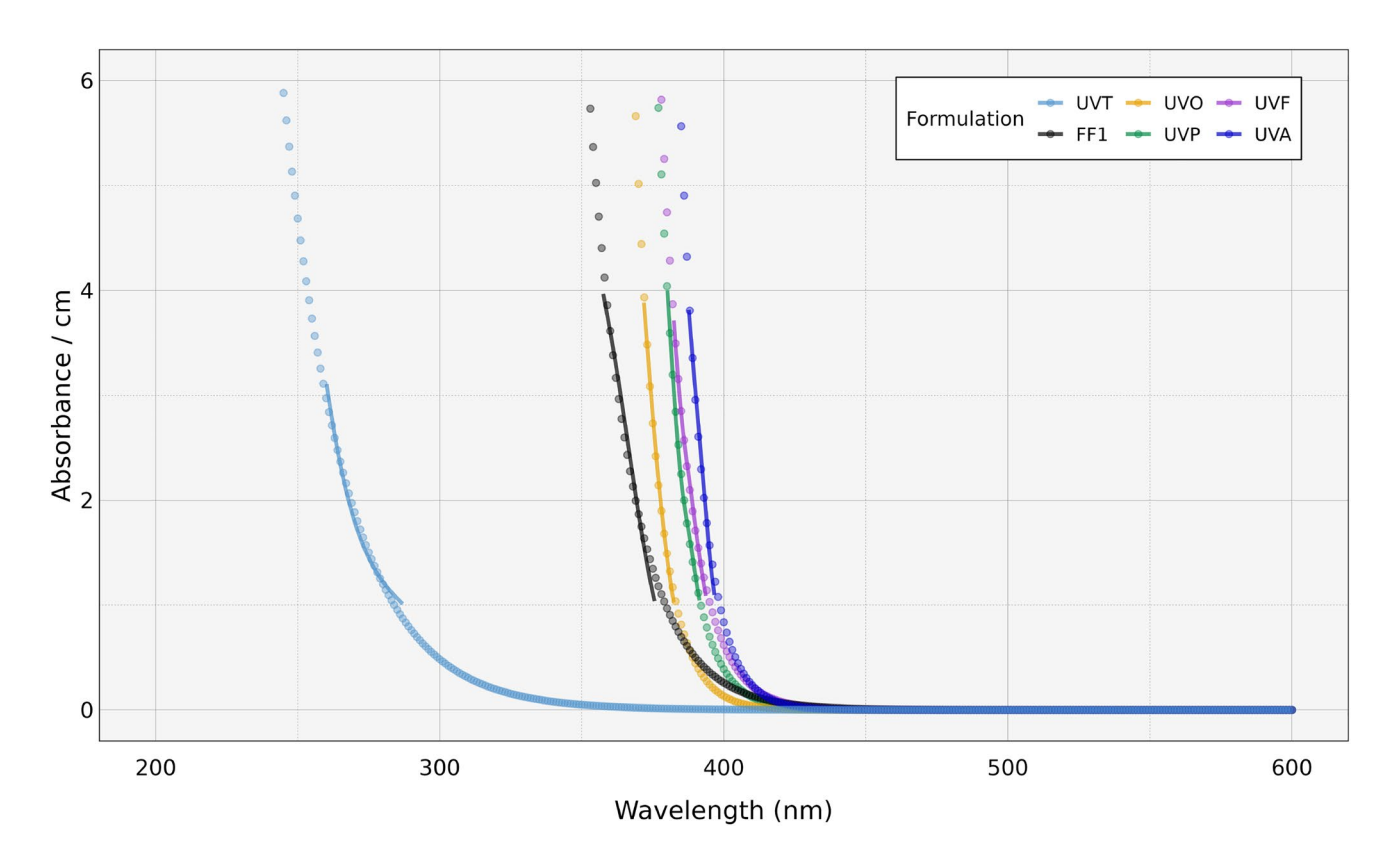


Fig. 7 Urbach fit analysis of PMMA samples prior to exposure

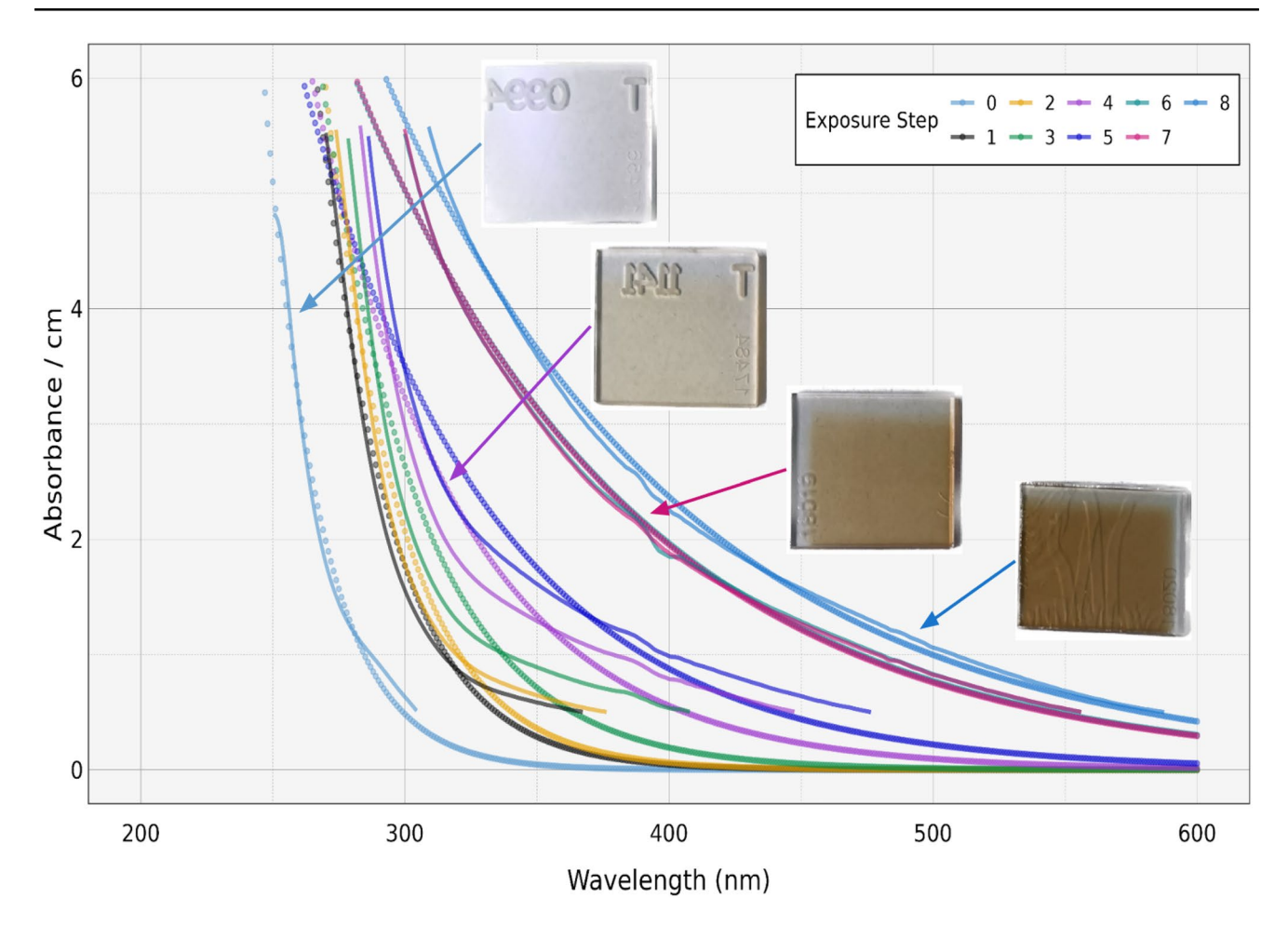


Fig. 8 The Urbach fit analysis of unstabilized UVT in Hot QUV

shown in particular because Hot QUV exposure conditions induce much higher yi values compared to other exposure conditions. UVT and FF1 samples result in a much higher yellowing compared to the rest of the PMMA samples.

Figure 10 shows the degradation pathway diagram generated from the netSEM-markovian model for UVT samples in Hot QUV exposure for three phases of degradation. The relationship between UV dose (uvadose) and yellowness index (YI) depicts the  $\langle Stressor \mid Response \rangle$  ( $\langle S \mid R \rangle$ ) relationship, which transitions from a change point behavior in Phase 1 to a quadratic behavior in Phase 2 and reverting back to a change point in Phase 3. Throughout the different phases, the adjusted  $R^2$  values remain significantly high, inferring a very good correlation between uvdose and YI. There is a high correlation in the relationship of IAD<sub>400</sub> with uvadose and YI across all three phases.

Interestingly, IAD<sub>275</sub>, which is related to the Fundamental Absorption Edge of PMMA, only has high correlation during Phase 1 for the relationships with uvadose and YI, trickling down to a low adjusted  $R^2$  value for Phases 2 and 3.

Similarly, the degradation pathway of FF1 samples can also be explored, as shown in Fig. 11. The difference between the degradation pathway for FF1 and UVT is the consideration of IAD $_{298}$  and IAD $_{339}$  in the degradation modeling, as FF1 contains Tinuvin P as a stabilizer. The relationship between uvadose and YI has a high correlation across all three phases. The relationship between IAD $_{400}$  and YI disappeared after Phase 1 and the relationship between IAD $_{275}$  and YI disappeared in Phase 2.

#### **Mechanical Characterization**

# **Surface Roughness**

The surface roughness of samples exposed in QSUN was initially investigated using optical profilometry for samples at exposure steps 0, 3, and 5 in QSUN exposure due to the high haze formation observed in step 5 samples. The haze formation in samples was observed as an opaque spot in the center of the backside of sample with the haze (%) value of the spot increasing with the increasing irradiance dosage, resulting in



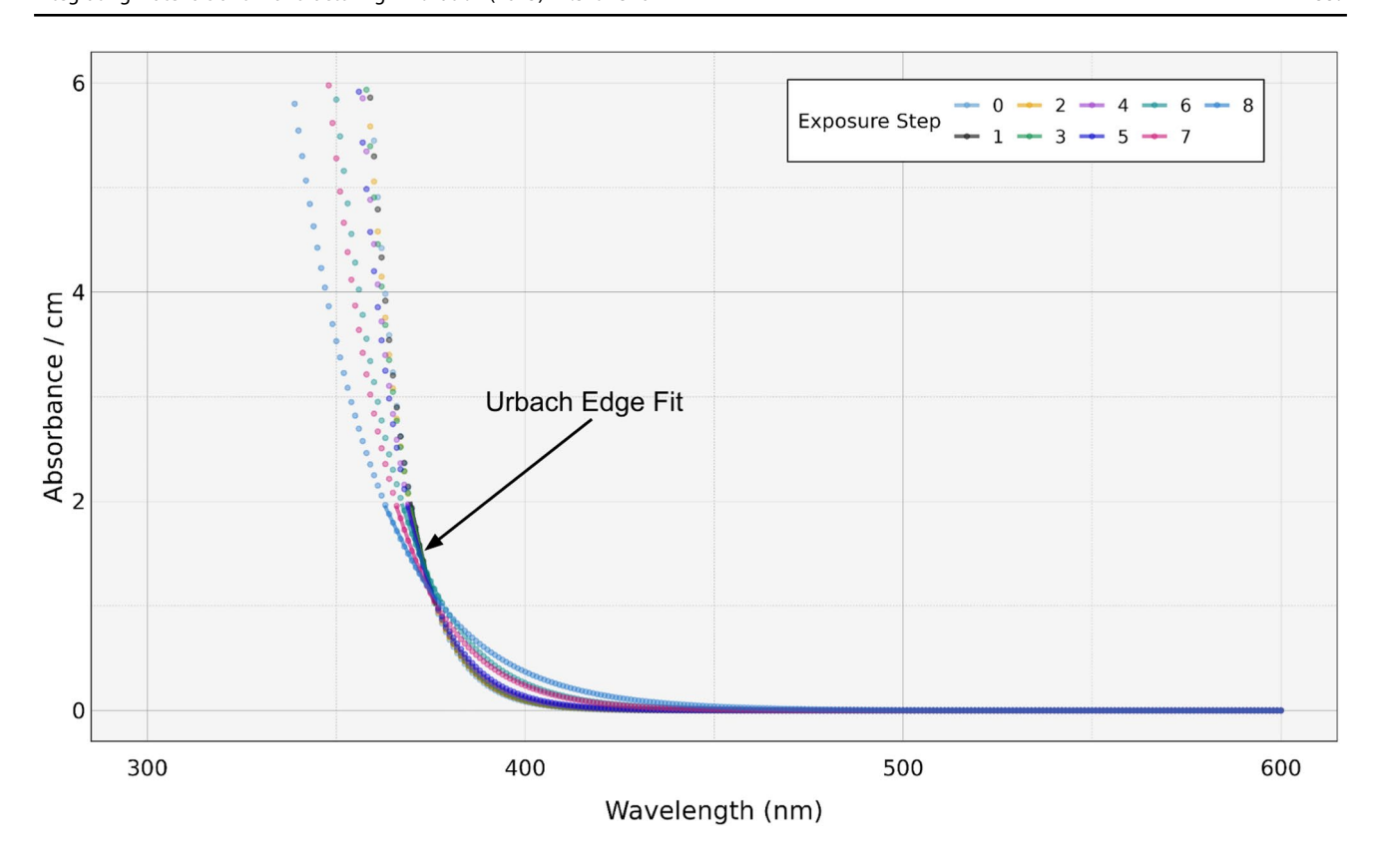


Fig. 9 The Urbach fit analysis of FF1 in Hot QUV

**Table 5** Urbach edge fit parameters for PMMA samples in Hot QUV at 0 h

PMMA formulation	Step	Exposure time (hour)	Urbach edge position (nm)	Urbach edge position (eV)	Urbach edge width (eV)
UVT	0	0	285	4.35	0.40
FF1	0	0	380	3.26	0.13
UVO	0	0	383	3.24	0.07
UVP	0	0	392	3.16	0.07
UVF	0	0	395	3.14	0.08
UVA	0	0	399	3.11	0.06

**Table 6** Urbach edge fit parameters for UVT samples in Hot QUV

PMMA formulation	Step	Exposure time (hour)	Urbach edge position (nm)	Urbach edge position (eV)	Urbach edge width (eV)
UVT	0	0	285	4.35	0.40
UVT	1	400	316	3.92	0.50
UVT	2	800	321	3.86	0.52
UVT	3	1200	337	3.68	0.67
UVT	4	2200	367	3.38	0.78
UVT	5	3200	391	3.17	0.83
UVT	6	16200	472	2.63	0.83
UVT	7	17400	471	2.63	0.82
UVT	8	22500	500	2.48	0.81



**Table 7** Urbach edge fit parameters for FF1 samples in Hot QUV

PMMA formulation	Step	Exposure time (hour)	Urbach edge position (nm)	Urbach edge position (eV)	Urbach edge width (eV)
FF1	0	0	376	3.30	0.08
FF1	1	400	377	3.29	0.09
FF1	2	800	376	3.30	0.09
FF1	3	1200	377	3.29	0.09
FF1	4	2200	377	3.29	0.10
FF1	5	3200	377	3.29	0.10
FF1	6	16200	378	3.28	0.14
FF1	7	17400	377	3.29	0.14
FF1	8	22500	378	3.28	0.20

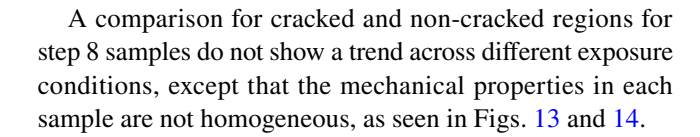
a visually observable spot by step 5 exposure. The roughness of the back side of the samples was observed to be higher than the irradiated front side, as shown in Fig. 12.

#### Microindentation

Cracks visually observed in the step 8 exposure were evaluated using microindentation. The effect of different exposure conditions on the mechanical properties of unstabilized UVT and stabilized FF1 samples for baseline 0 and 8 exposure steps were assessed by measurements of stiffness and surface hardness of the sample using Young's modulus and Vickers hardness.

As illustrated in Figs. 13 and 14, a higher Young's modulus and Vickers hardness was observed for baseline stabilized FF1 samples comparatively to unstabilized baseline UVT samples. Comparing between the two exposure steps, samples at step 8 for both FF1 and UVT show a statistically significant decrease in Young's modulus, with the exception of HQUV exposure condition for UVT samples. In addition, a larger decrease in Young's modulus for FF1 samples compared to that of UVT samples can be observed in Cyclic QUV (CQUV) and Hot QUV (HQUV). Nevertheless, FF1 samples in QSUN exposure still maintain higher Young's modulus values than UVT samples. There was also no statistically significant difference between Young's modulus values for CQUV and HQUV exposure conditions for both step 8 UVT and FF1 samples.

For Vickers hardness, all step 8 samples for FF1 show a statistically significant decrease for all exposure conditions, while there was no difference for samples with UVT formulation. There was also no statistically significant difference in Vickers hardness between HQUV and CQUV exposure conditions for FF1 and UVT samples in step 8. However, FF1 samples have lower values of Vickers hardness than that of UVT samples in HQUV exposure, but are more or less the same for CQUV and QSUN exposure conditions.



# **Discussion**

# **Acrylic Degradation Study Protocol**

A study protocol involving the exposure of varying PMMA formulations to different exposure conditions with a varying combination of known degradation stressors allow us to study the synergistic affect as well as the isolated contribution of degradation from stressors. The rate of degradation can be compared for UV and full spectrum light exposure or the presence of moisture. In addition, investigating varying combinations of PMMA formulations, with one unstabilized formulation set as a control, shows the impact of protective additives on the rate of degradation. A stepwise exposure and evaluation provides higher resolution to track changes in samples that could otherwise be overlooked in a holistic exposure evaluated at the final exposure step.

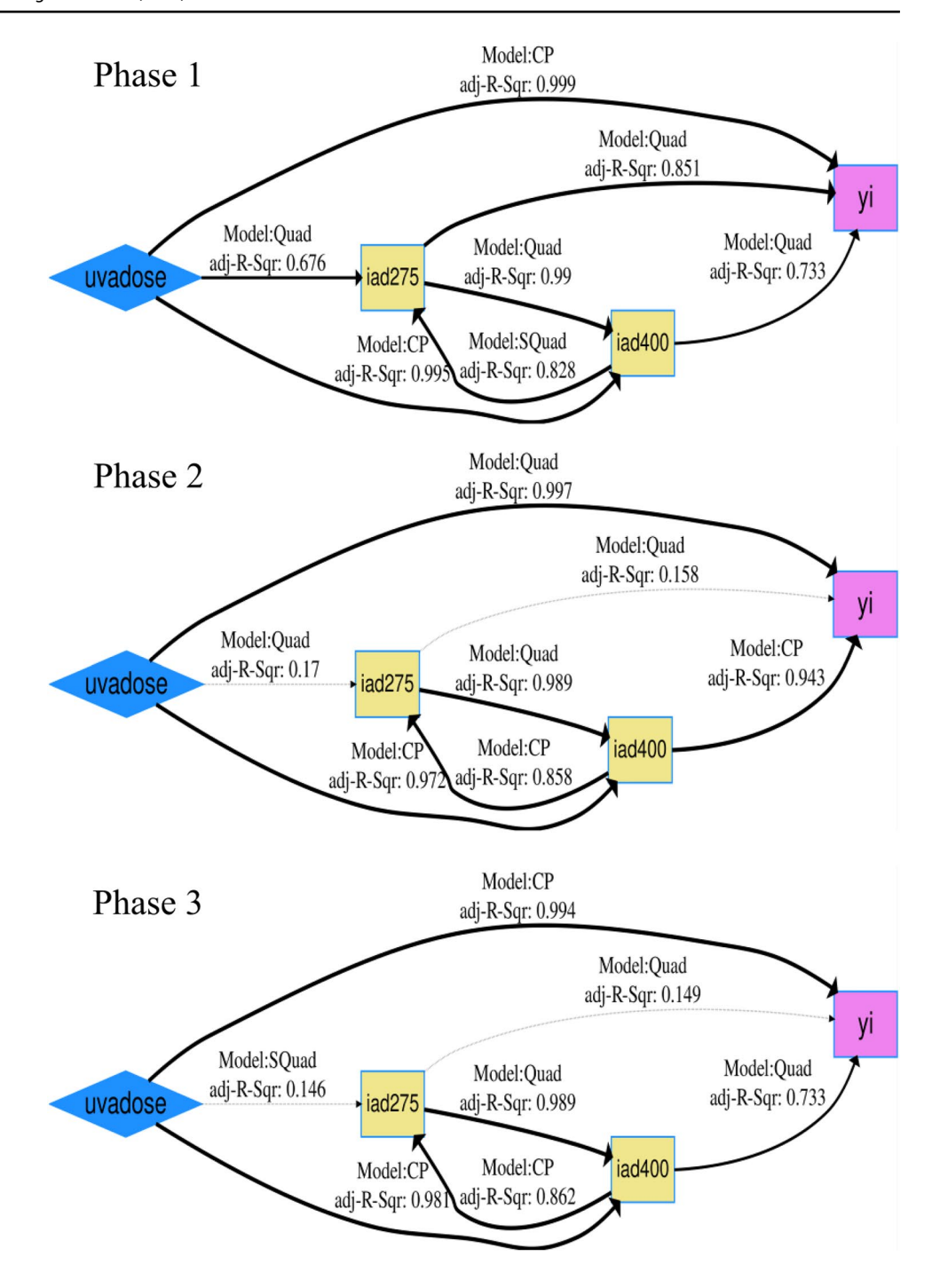
# Effect of Exposures on Degradation of PMMA Chemical Properties

Discoloration or yellowing is one of the main performance losses in PMMA occurring from the photodegradation. PMMA can undergo photooxidation caused by free radical formation induced by UV. The methylmethacrylate is converted into a peroxyl radical species, which can impact the polymer backbone structure [5, 58–60].

Samples exposed in Hot QUV exposure had a much higher YI compared to samples in other exposures. Hot QUV has the largest amount of accumulated UVA-340 dosage compared to other exposure conditions. In addition, the synergistic effect of temperature and UV irradiation may



Fig. 10 Comparison of Phases in Acrylic Degradation for unstabilized UVT samples using Inferential (Markovian) Model from netSEM. CP indicates change point model. Quad indicates Quadratic model. Phase 1 is modeled using data from step 0–5. Phase 2 is modeled using data from step 0–7. Phase 3 is modeled using data from step 0–8



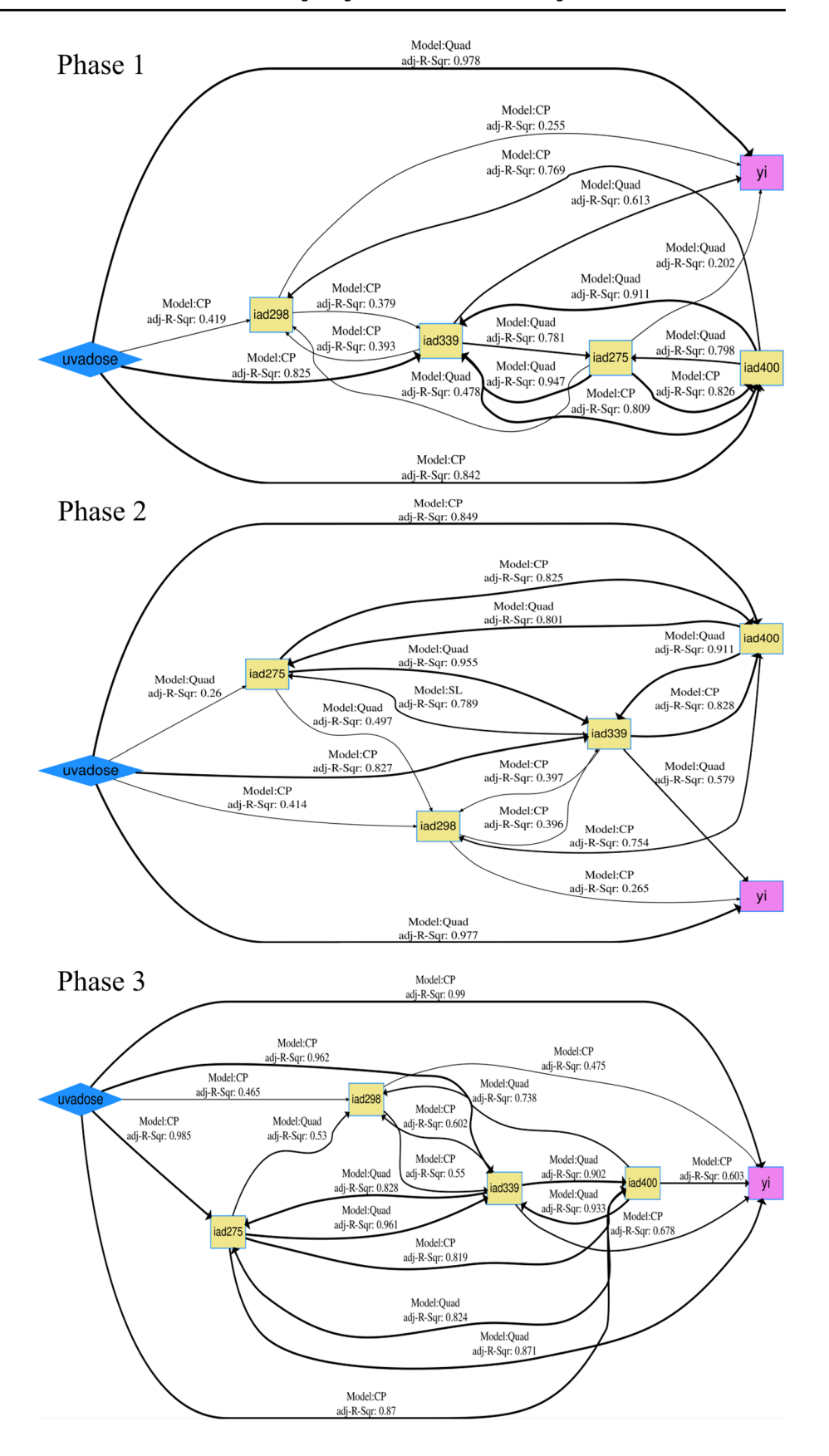
also account for the highest yellowing rate observed in the highly intensified exposure in Hot QUV. Photolytic degradation of PMMA occurring around wavelengths 300–330 nm could be due to the absorbance from ester groups and potentially carbonyl groups [5] or initiated from ketones and hydroperoxides that radicalize more efficiently for the given wavelength range [61]. This explains why samples have the lowest YI values in QSUN exposure which uses full spectrum light. Thermal degradation in PMMA gains significance at temperatures above 150 °C [30]. Since the

temperature for exposure conditions is around 70 °C, thermal degradation is less apparent compared to photolytic degradation.

The rate of degradation can also be observed in the IAD spectrum. Unstabilized UVT samples, which have higher YI values than FF1 samples, also have much higher IAD values. In FF1 samples, the negative IAD values around 298 and 339 nm show the bleaching of Tinuvin P UV absorber as the samples go through degradation. This shows that Tinuvin P



Fig. 11 Comparison of phases in acrylic degradation for stabilized FF1 samples using Inferential (Markovian) Model from netSEM. CP indicates change point model. Quad indicates Quadratic model. Phase 1 is modeled using data from step 0–5. Phase 2 is modeled using data from step 0–7. Phase 3 is modeled using data from step 0–8





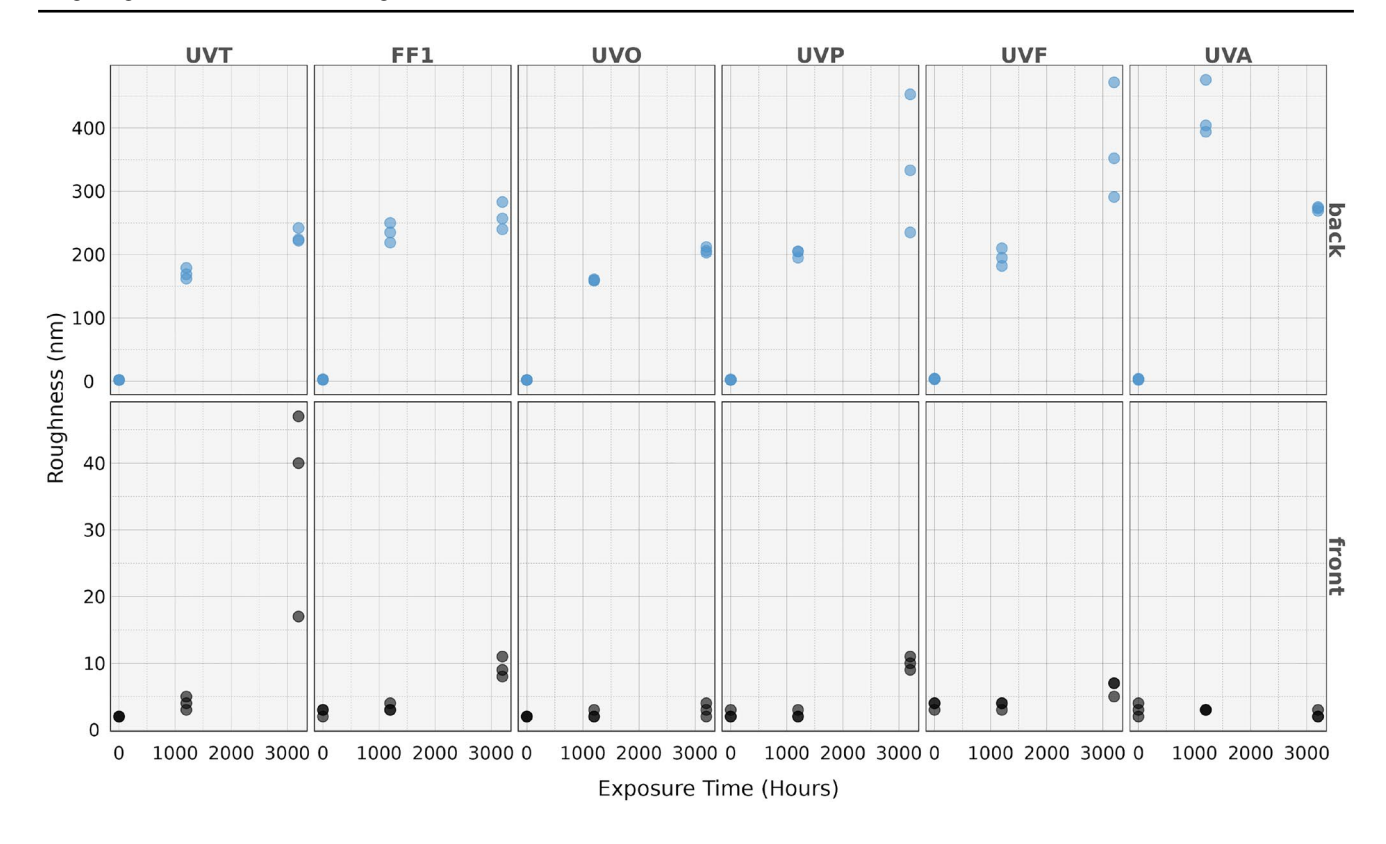


Fig. 12 Surface roughness of irradiated side (front) and non-irradiated side (back) of samples in QSUN

is being sacrificed in order to the protect the samples from degradation.

The negative IAD values could also result from the dissolution of chromophores through hydrolysis. The removal of degraded compounds from the surface has been shown in thin PET films after the films were placed in deionized (DI) water following accelerated exposure conditions [62]. To confirm the removal of degraded products from the surface of degraded acrylic samples through the action of water would require an exposure condition with the combination of UV light exposure and water spray. Additionally, the IAD values calculated from UV–Vis-NIR measurements characterize the chemical changes throughout the bulk of acrylic sample. Therefore, the IAD values would not inform about changes at the surface level of the acrylic samples.

We also observed that the Urbach edge position for UVT samples shifted toward a longer wavelength as it goes through degradation. The shift is due to the formation of degradation by-products in the polymer matrix [63]. The Urbach edge position is also related to the yellowing of the sample for UVT formulation, as shown in Fig. 8. The sample gets more yellow as the absorbance increases in the visible wavelength region around 400 nm, which indicates that blue light is being absorbed. Compared to UVT, FF1 samples, which contain additives, barely shift in Urbach

edge position. This suggests that the role of the light stabilizers prevent degradation, therefore mitigating changes in PMMA's optical properties. To observe whether the acrylic samples are exhibiting by-product formation on or near the surface, we performed analysis using an ATR-FTIR spectroscopy. It is understood that by-products like anhydrides can form from acrylic degradation [64]. We observed, for example, in samples containing the FF1 formulation under CQUV exposure conditions that strong peaks owing to the C=O stretch from anhydrides occurring around 1820-1750 cm<sup>-1</sup> are not present in all exposure steps. This suggests that by-products like methacrylic and acrylic anhydrides do not form near or on the surface of the acrylic samples. In order to investigate if these and other by-products form within the samples, destructive tests will need to be performed in future work (Fig. 15).

# Effect of Exposures on Degradation of PMMA Mechanical Properties

### **Investigation of Haze Formation**

Surface roughness of samples exposed in QSUN exposure was evaluated to investigate the haze formation at the back side of the samples. The changes in surface roughness for samples from steps 0 to 5 in QSUN exposure is most likely



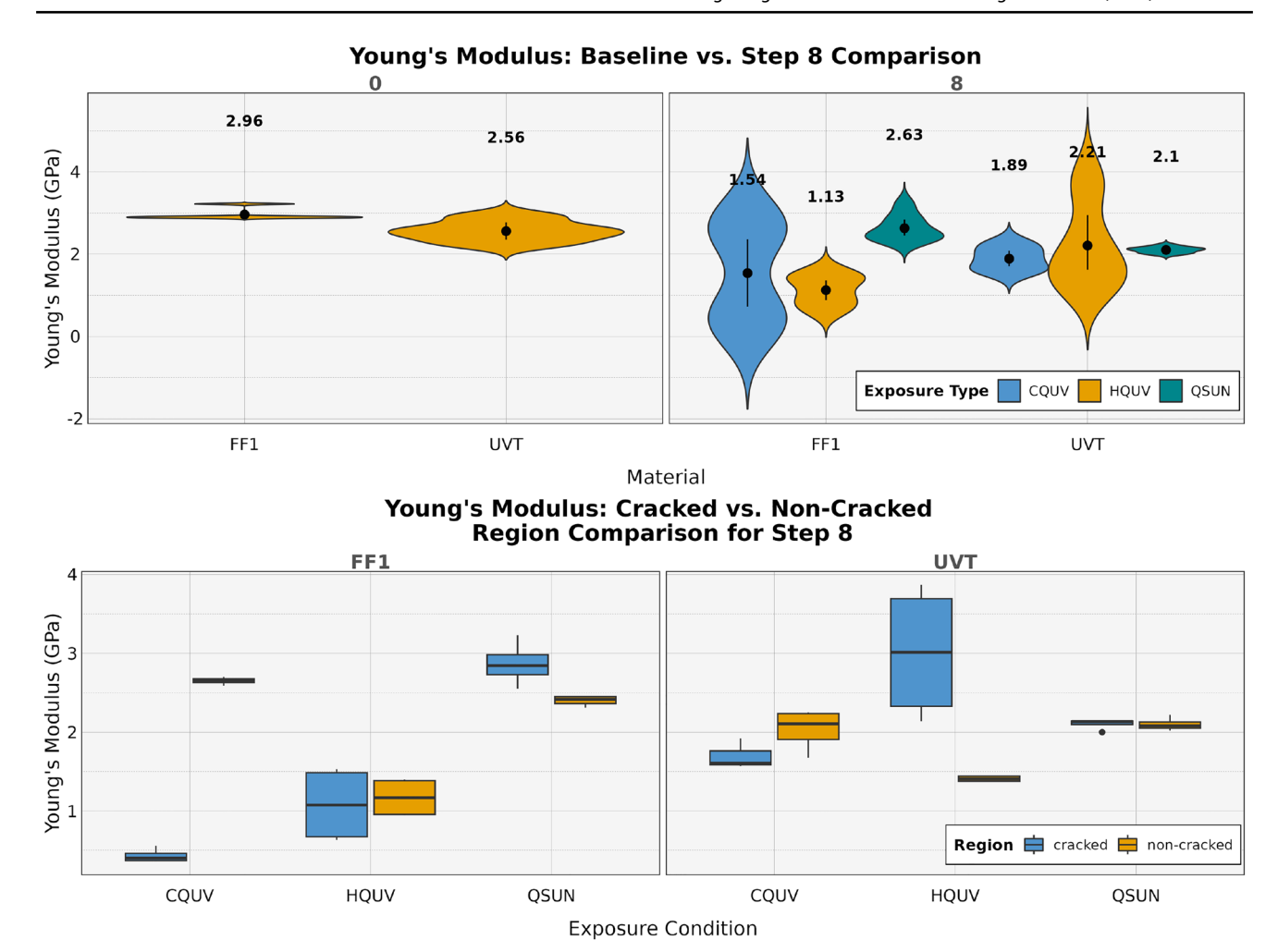


**Fig. 13** Left: Comparison of Young's modulus between baseline (Step 0) and step 8 samples for unstabilized UVT and stabilized FF1 formulations. Error bars indicate 83.4 % confidence interval. Right:

Comparison of Young's modulus between cracked and non-cracked region of sample for step 8 exposure for different exposure conditions: HQUV, CQUV, and QSUN

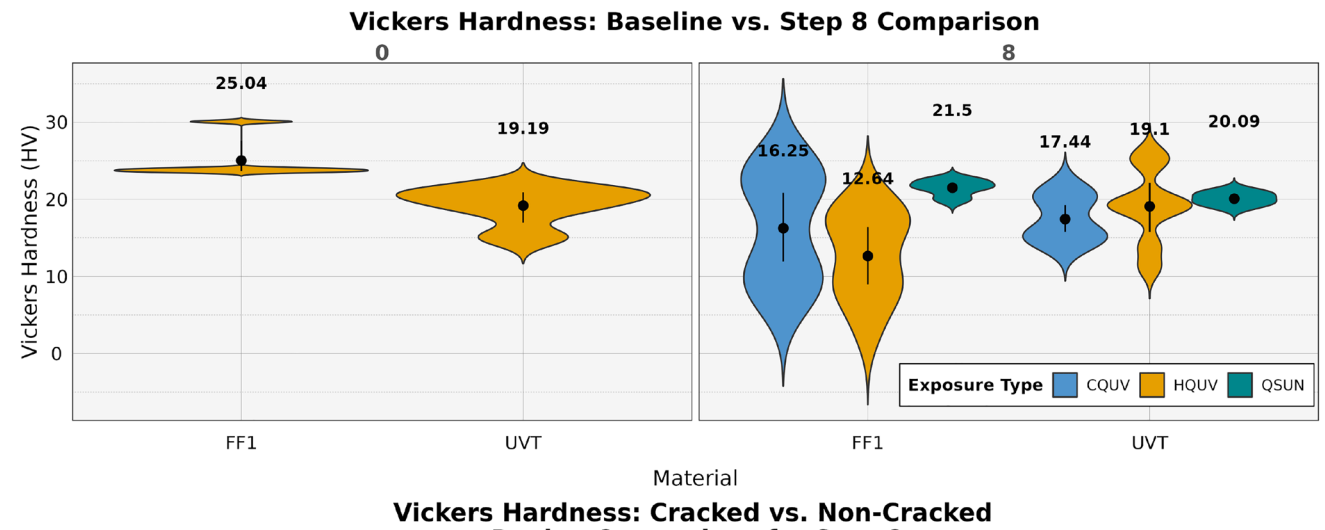
related to interaction between the residual water from QSUN water spray cycle and the backside of PMMA samples. The residual water on the backside cannot totally evaporate during the 102-minute full spectrum light-only exposure cycle in QSUN, which means that the center of backside of samples in QSUN is in contact with water all the time during the 3200 h of exposure. That fact can explain why there are more haze formations in the center of the backside of PMMA sample in QSUN compared to samples in other exposure conditions. Consequently, it can be inferred that the combination of moisture and full-spectrum light exposure with the inability for water to evaporate are the main stress conditions that lead to the significant haze formation as opposed to the combination of moisture and UV exposure.

#### **Investigation of Crack Formation**

The Young's modulus and Vickers hardness were evaluated using microindentation to investigate the conditions behind crack formation in PMMA samples. Samples from baseline (step 0) and step 8 exposures were measured to compare the changes in mechanical properties, as cracks were visually observed on the samples by step 8 exposure. UVT unstabilized and FF1 stabilized samples were measured in particular to investigate the presence of additives on the degradation of mechanical properties, especially since these samples showed the highest degree of cracking compared to other PMMA formulations.

A higher Young's modulus (stiffer) and Vickers hardness values found in baseline FF1 samples (step 0) in comparison to UVT samples could be attributed to the presence of additives in FF1 samples. As the samples undergo degradation after being exposed to different exposure





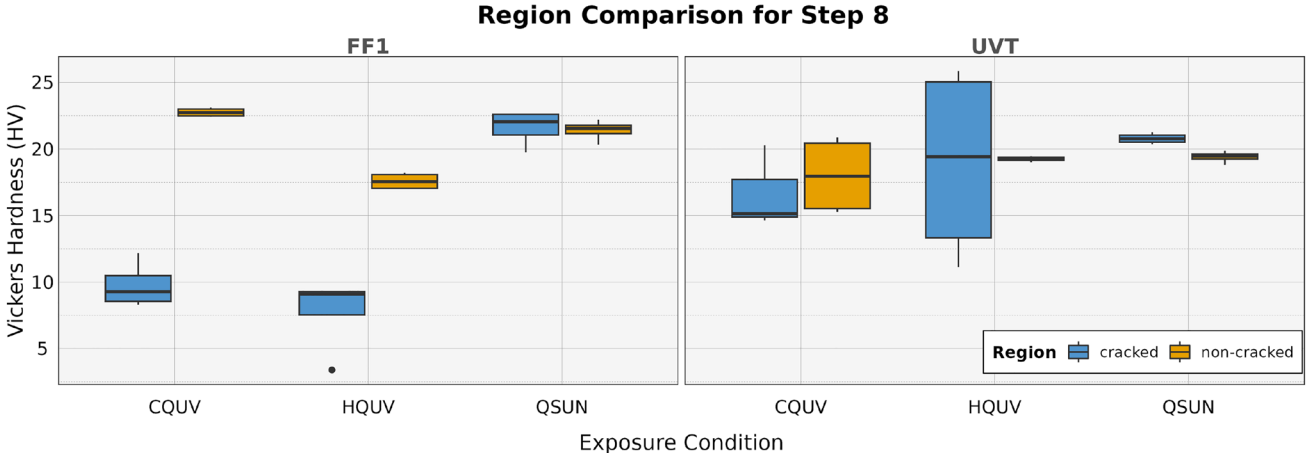


**Fig. 14** Top: Comparison of surface hardness (Vickers hardness) between baseline (step 0) and step 8 samples for unstabilized UVT and stabilized FF1 formulations. Error bars indicate 83.4% confidence interval. Bottom: Comparison of surface hardness (Vickers

hardness) between cracked and non-cracked region of sample for step 8 exposure for different exposure conditions: HQUV, CQUV, QSUN

conditions, a decrease in Young's modulus and Vickers hardness is observed, especially for FF1 samples in Hot QUV and Cyclic QUV exposure conditions.

Chain scission has been shown to be the main mechanism of photodegradation in PMMA, which could explain the reduction in Young's modulus of samples, as polymer chains get broken up, which reduces the stiffness of the polymer matrix [65]. Additionally, in the presence of moisture, water can penetrate the acrylic matrix, acting as a plasticizer. Within the matrix, water molecules can mitigate hydride abstraction of the acrylic backbone by increasing the void volume of the adjacent chains, making it difficult to form cross-linking networks due to increased distance between the chains [66].

However, unlike what was observed by Babo et al. [65], an increasing surface hardness with decreasing molecular weight, we observed a decreasing surface hardness of the

PMMA samples. The decrease in surface hardness could be due to water molecules acting as a plasticizer, especially in a Cyclic QUV exposure condition, which contains a condensing humidity cycle. Samples in QSUN exposure, which are exposed to full spectrum light and water spray, do not show much reduction in Young's modulus and surface hardness. This infers the importance of UV as the main stress factor to the degradation of PMMA samples. It is interesting to observe that FF1 samples presented greater decrease in Young's modulus and surface hardness compared to UVT samples, as it was expected that stabilized FF1 samples would be less degraded than unstabilized UVT samples.



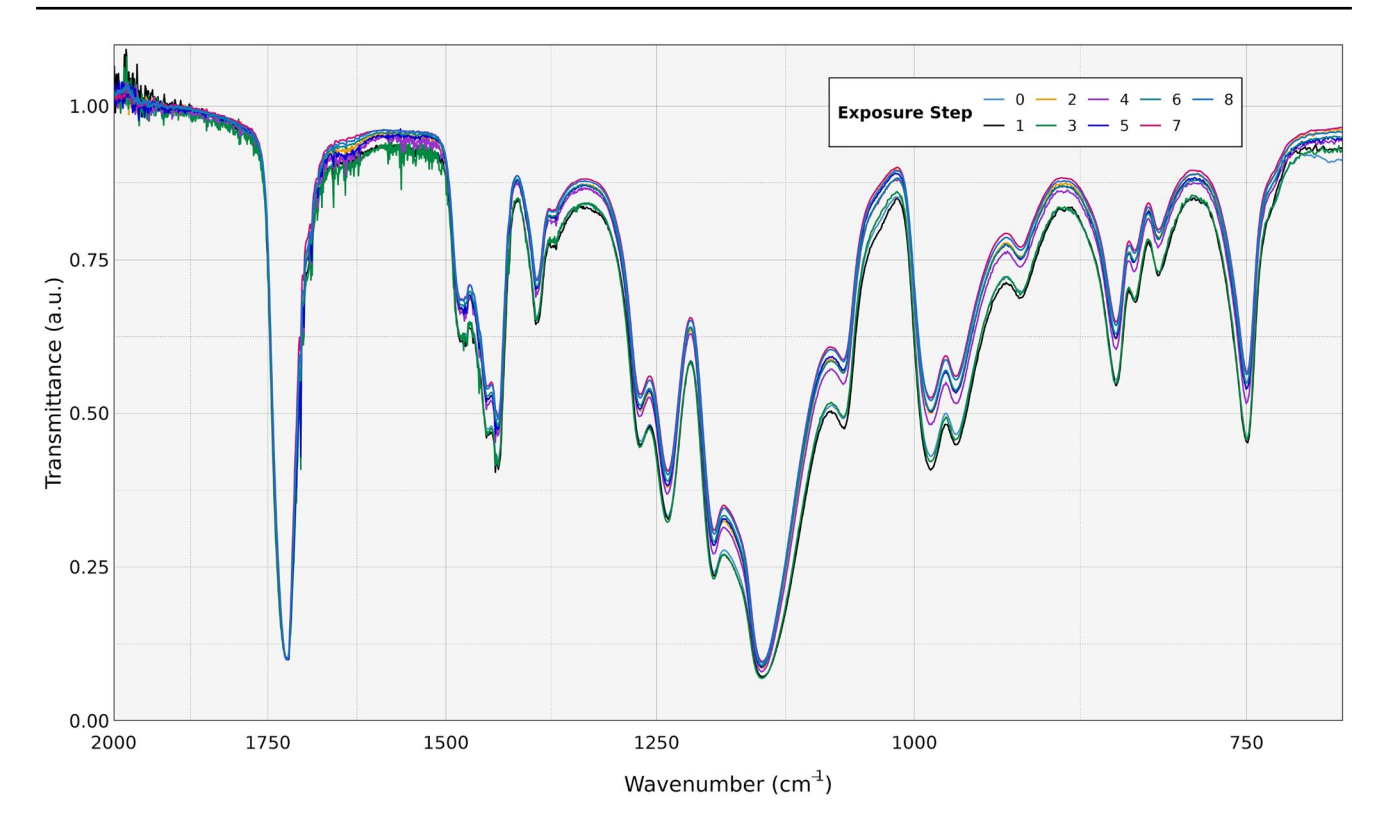


Fig. 15 FTIR spectrum from 700 to 2000 cm<sup>-1</sup> for FF1 formulation under Cyclic QUV exposure

### **Degradation Pathway Models of PMMA**

The netSEM-markovian model on different subsets of the exposure steps of PMMA samples shows changes in behavior of relationship between variables as well as the strength of the relationship (changes in adjusted  $R^2$ ). The three different phases observed visually in the samples as well as modeled using the netSEM-markovian model indicate the three different phases of degradation in PMMA [37]:

- Stage 1 Bleaching of UV stabilizers.
- Stage 2 Breaking of Acrylic backbone structure.
- Stage 3 Degradation of mechanical Properties.

The degradation pathways from the pathway diagrams generated from netSEM can be interpreted by following along the path of higher adjusted  $R^2$  from  $\langle S | R \rangle$ ,  $\langle S | M \rangle$ , and  $\langle M | R \rangle$ . For instance, in the degradation pathway diagram for UVT samples in HQUV exposure, a high adjusted  $R^2$  value from uvadose to YI in all three phases infers the significance of uvadose in the yellowing failure mode of the samples across all three phases. The change in adjusted  $R^2$  for the relationship of uvadose and IAD<sub>275</sub> from 0.676 in Phase 1 to 0.17 in Phase 2 and 0.146 in Phase 3 suggests that the fundamental absorbance edge

of PMMA was only significantly affected by UV in the first phase of degradation. Similarly, we observed the decrease in adjusted  $R^2$  for the relationship of IAD<sub>275</sub> and YI from Phase 1 to Phase 3 suggesting the decreasing significance of the fundamental absorbance edge to the yellowing of the samples as the exposure continues. In contrast, the relationship between uvadose and IAD<sub>400</sub> and IAD<sub>400</sub> and YI has been observed to have a high adjusted  $R^2$  in all three Phases which suggests the significance of the formation of chromophores from UV degradation leading to yellowing of samples in all three degradation phases.

The changes in netSEM-markovian degradation pathway diagrams are more apparent in the case of FF1 samples. In Phase 1 we can observe that there is a low adjusted  $R^2$  value (0.202) for IAD<sub>275</sub> to YI and no relationship for IAD<sub>400</sub> to YI. Additionally, IAD<sub>298</sub> and IAD<sub>339</sub> have direct relationship from uvadose and IAD<sub>339</sub>, in particular, have high adjusted  $R^2$  value with YI. This infers the active role of UV stabilizers in FF1 samples to prevent the samples from changes in fundamental absorbance edge and yellowing. As we move to Phase 2 and Phase 3, we can observe the changes in the pathway diagram that infers degradation starting to take place and stabilizers being depleted. In Phase 2, we start to observe the direct relationship between uvadose and IAD<sub>275</sub> inferring the changes in fundamental absorbance edge due to UV light. In Phase 3, we observe that the



relationship between IAD<sub>400</sub> and YI has been established with an adjusted  $R^2$  of 0.603 suggesting the significance of chromophore formation to yellowing of samples.

# **Conclusion**

A domain knowledge-based and data-driven approach was utilized to quantitatively investigate the temporal evolution of degradation modes, mechanisms, and rates under various stepwise exposure conditions in PMMA. The impact of additives and different exposure conditions on the degradation of PMMA was investigated using a study protocol involving six formulations of PMMA with different combinations of UV additives exposed under three weathering conditions with various combinations of stress factors.

Evaluation of yellowness index as a performance metric highlighted the performance of additives as the unstabilized samples showed much higher YI values compared to stabilized samples. UVA-340 was also found to be more damaging to PMMA samples than full spectrum light regardless of the presence of moisture inferring the wavelength dependency in the degradation process. A shift in Urbach edge toward longer wavelengths was found to be consistent with the degradation of samples, as the absorbance around 400 nm wavelength increases with the increase in yellowing of samples. The use of Induced Absorbance to Dose to track degradation mechanisms allowed the comparison of degradation rates across different PMMA formulations and exposure conditions.

netSEM modeling showed the transition in the degradation phases of PMMA, which was also visibly observed as the samples eventually increase in yellowing and begin to crack. This informs the consideration of temporal change in mechanical properties during degradation for future studies, which could be conducted using the retained samples. The degradation pathway diagram with netSEM also allows inference for which degradation mechanism could take precedence over others from the strength of adjusted  $R^2$  between relationships in a <Stressor | Mechanism | Response> framework. A degradation science study protocol approach, along with degradation modeling informed by a *<Stressor* | Mechanism | Response> framework, is a useful tool for exploring and understanding degradation mechanisms in a weathering study.

Acknowledgements This research was performed at the SDLE Research Center, which was established through funding by the Ohio Third Frontier, Wright Project Program Award tech 12-004. This work made use of the Rider High Performance Computing Resource in the Core Facility for Advanced Research Computing at Case Western Reserve University. Micro-indentation measurements were performed

at the CWRU Materials for Opto/electronics Research and Education (MORE) Center, a CWRU core facility est. 2011 via Ohio Third Frontier grant TECH 09-021. This material is based upon work supported by the U.S. National Science Foundation Award EEC-2052776 and EEC-2052662 in the MDS-Rely IUCRC Center, under the NSF Solicitation: NSF 20-570 Industry-University Cooperative Research Centers Program (H.H.A, L.S.B). This material is based upon research in the Materials Data Science for Stockpile Stewardship Center of Excellence (MDS3-COE), and supported by the Department of Energy's National Nuclear Security Administration under Award Number(s) DE-NA0004104 (R.H.F and J.C.J). This work was performed, in part, under the auspices of the U.S. Department of Energy by Lawrence Livermore National Laboratory under Contract DE-AC52-07NA27344, LLNL-JRNL-853607-DRAFT (J.C.J). The views expressed herein do not necessarily represent the views of the U.S.Department of Energy or the United States Government.

#### **Declarations**

**Conflicts of interest** On behalf of all authors, the corresponding author states that there is no conflict of interest.

# References

- Yang HE, French RH, Bruckman LS (eds) (2019) Durability and reliability of polymers and other materials in photovoltaic modules, 1st edn. Elsevier, William Andrew Applied Science Publishers, Amsterdam. https://doi.org/10.1016/C2016-0-01032-X
- Campo EA (2007) Industrial polymers. Hanser Publications, Middletown, OH
- Kurr F (2015) Handbook of plastics failure analysis (eBook). Hanser Publications, Middletown, OH
- Gupta A, Liang R, Tsay FD, Moacanin J (1980) Characterization of a dissociative excited state in the solid state: photochemistry of Poly(methyl methacrylate). Photochemical processes in polymeric systems.
   Macromolecules 13(6):1696–1700. https://doi.org/10.1021/ma60078a060
- Dickens B, Martin JW, Waksman D (1984) Thermal and photolytic degradation of plates of poly(methyl methacrylate) containing monomer. Polymer 25(5):706–715. https://doi.org/10.1016/0032-3861(84)90041-7
- 6. Allen NS, Edge M (1992) Fundamentals of polymer degradation and stabilisation. Elsevier Applied Science, London
- Ali U, Karim KJBA, Buang NA (2015) A review of the properties and applications of poly (methyl methacrylate) (PMMA). Polym Rev 55(4):678–705. https://doi.org/10.1080/15583724. 2015.1031377
- D4802 A. ASTM D4802 10 standard specification for poly(methyl methacrylate) acrylic plastic sheet
- Harper CA (2000) Modern plastics handbook, 1st edn. McGraw-Hill Education, New York
- Frazer RQ, Byron RT, Osborne PB, West KP (2005) PMMA: an essential material in medicine and dentistry. J Long-term Eff Med Implants. https://doi.org/10.1615/JLongTermEffMedImplants.v15.i6.60
- Koh Y, Jang S, Kim J, Kim S, Ko YC, Cho S, Sohn H (2008) DBR PSi/PMMA composite materials for smart patch application. Colloids Surf A Physicochem Eng Asp 313–314:328–331. https://doi.org/10.1016/j.colsurfa.2007.04.103
- Chakraborty H, Sinha A, Mukherjee N, Ray D, Protim Chattopadhyay P (2013) A study on nanoindentation and tribological behaviour of multifunctional ZnO/PMMA nanocomposite.



- Mater Lett 93:137–140. https://doi.org/10.1016/j.matlet.2012. 11.075
- Thomas P, Ernest Ravindran RS, Varma KBR (2014) Structural, thermal and electrical properties of poly(methyl methacrylate)/CaCu<sub>3</sub>Ti<sub>4</sub>O<sub>12</sub> composite sheets fabricated via melt mixing. J Therm Anal Calorim 115(2):1311–1319. https://doi.org/10.1007/s10973-013-3500-x
- Wu H, Ma G, Xia Y (2004) Experimental study of tensile properties of PMMA at intermediate strain rate. Mater Lett 58(29):3681–3685. https://doi.org/10.1016/j.matlet.2004.07.022
- El-Bashir SM, Al-Harbi FF, Elburaih H, Al-Faifi F, Yahia IS (2016) Red photoluminescent PMMA nanohybrid films for modifying the spectral distribution of solar radiation inside greenhouses. Renew Energy 85:928–938. https://doi.org/10. 1016/j.renene.2015.07.031
- Hammam M, El-Mansy MK, El-Bashir SM, El-Shaarawy MG (2007) Performance evaluation of thin-film solar concentrators for greenhouse applications. Desalination 209(1):244–250
- Yang L, Zhou S, Wu L (2015) Preparation of waterborne selfcleaning nanocomposite coatings based on TiO<sub>2</sub>/PMMA latex. Prog Org Coat 85:208–215. https://doi.org/10.1016/j.porgcoat. 2015.04.012
- Bora MÖ (2014) The influence of heat treatment on scratch behavior of polymethylmethacrylate (PMMA). Tribol Int Complet 78:75–83. https://doi.org/10.1016/j.triboint.2014.04.030
- Hamouda AMS (2002) The influence of humidity on the deformation and fracture behaviour of PMMA. J Mater Process Technol 124(1):238–243. https://doi.org/10.1016/S0924-0136(02)00096-1
- Jaiganesh V, Christopher A, Mugilan E (2014) Manufacturing of PMMA cam shaft by rapid prototyping. Proced Eng 97:2127– 2135. https://doi.org/10.1016/j.proeng.2014.12.456
- Moghbelli E, Banyay R, Sue H-J (2014) Effect of moisture exposure on scratch resistance of PMMA. Tribol Int 69:46–51. https://doi.org/10.1016/j.triboint.2013.08.012
- Arndt T, Richter S, Pasierb M (2013) Accelerated laboratory weathering of acrylic lens materials. AIP Conf Proc 1556(1):218– 221. https://doi.org/10.1063/1.4822235
- Pickett JE, Moore JE (1993) Photodegradation of UV screeners. Polym Degrad Stab 42(3):231–244. https://doi.org/10.1016/0141-3910(93)90219-9
- Pickett JE, Moore JE (1996) Photostability of UV screeners in polymers and coatings. ACS Publications, Washington, pp 287–301. https://doi.org/10.1021/ba-1996-0249.ch019
- Hamid SH (2014) Handbook of polymer degradation, 2nd edn. CRC Press, Boca Raton. https://doi.org/10.1201/9781482270181
- Gerlock JL, Smith CA, Núñez EM, Cooper VA, Liscombe P, Cummings DR, Dusibiber TG (1996) Measurements of Chemical change rates to select superior automotive clearcoats. ACS Publications, Washington, pp 335–347. https://doi.org/10.1021/ ba-1996-0249.ch022
- Chang TC, Yu PY, Hong YS, Wu TR, Chiu YS (2002) Effect of phenolic phosphite antioxidant on the thermo-oxidative degradation of PMMA. Polym Degrad Stab 77(1):29–34. https://doi.org/ 10.1016/S0141-3910(02)00076-9
- Troitskii BB, Troitskaya LS, Yakhnov AS, Dmitriev AA, Anikina LI, Denisova VN, Novikova MA (2000) Temperature limit of inhibition of thermo- oxidative degradation of polystyrene and poly(methyl methacrylate) by antioxidants. Int J Polym Mater Polym Biomater 46(1–2):315–330. https://doi.org/10.1080/00914 030008054864
- Vlachopoulos J, Strutt D (2003) Polymer processing. Mater Sci Technol 19(9):1161–1169. https://doi.org/10.1179/0267083032 25004738
- Fox RB, Isaacs LG, Stokes S (1963) Photolytic degradation of poly(methyl methacrylate). J Polym Sci Part A Gen Pap 1(3):1079–1086. https://doi.org/10.1002/pol.1963.100010321

- 31. Semen J, Lando JB (1969) The acid hydrolysis of isotactic and syndiotactic poly(methyl methacrylate). Macromolecules 2(6):570–575. https://doi.org/10.1021/ma60012a003
- Hirata T, Kashiwagi T, Brown JE (1985) Thermal and oxidative degradation of poly(methyl methacrylate): weight loss. Macromolecules 18(7):1410–1418. https://doi.org/10.1021/ma001 49a010
- Kashiwagi T, Hirata T, Brown JE (1985) Thermal and oxidative degradation of poly(methyl methacrylate) molecular weight. Macromolecules 18(2):131–138. https://doi.org/10.1021/ma00144a003
- 34. Manring LE (1991) Thermal degradation of poly(methyl methacrylate). 4. Random side-group scission. Macromolecules 24(11):3304–3309. https://doi.org/10.1021/ma00011a040
- Torikai A, Hattori T, Eguchi T (1995) Wavelength effect on the photoinduced reaction of polymethylmethacrylate. J Polym Sci Part A Polym Chem 33(11):1867–1871. https://doi.org/10.1002/ pola.1995.080331114
- Kaczmarek H, Kamińska A, Herk A (2000) Photooxidative degradation of poly(alkyl methacrylate)s. Eur Polym J 36(4):767–777. https://doi.org/10.1016/S0014-3057(99)00125-1
- French RH, Podgornik R, Peshek TJ, Bruckman LS, Xu Y, Wheeler NR, Gok A, Hu Y, Hossain MA, Gordon DA, Zhao P, Sun J, Zhang G-Q (2015) Degradation science: mesoscopic evolution and temporal analytics of photovoltaic energy materials. Curr Opin Solid State Mater Sci 19(4):212–226. https://doi.org/ 10.1016/j.cossms.2014.12.008
- Committee AG (2023) ASTM G154–23: standard practice for operating fluorescent ultraviolet (UV) lamp apparatus for exposure of materials, vol. ASTM G154–23. https://doi.org/10.1520/ G0154-23
- Committe A (2023) ASTM G155–23: standard practice for operating xenon arc lamp apparatus for exposure of materials, vol. ASTM G155–23. https://doi.org/10.1520/G0155-21
- Venkat SN, Yu X, Liu J, Wegmueller J, Jimenez JC, Barcelos EI, Aung HH, Li X, Jaubert J-N, French RH, Bruckman LS (2023) Statistical analysis and degradation pathway modeling of photovoltaic minimodules with varied packaging strategies. Front Energy Res. https://doi.org/10.3389/fenrg.2023.1127796
- Gok A, Fagerholm CL, French RH, Bruckman LS (2019) Temporal evolution and pathway models of poly(ethylene-terephthalate) degradation under multi-factor accelerated weathering exposures. PLoS One. https://doi.org/10.1371/journal.pone.0212258
- Murray MP, Bruckman LS, French RH (2012) Photodegradation in a stress and response framework: poly(methyl methacrylate) for solar mirrors and lens. J. Photon. Energy 2(1):022004. https://doi. org/10.1117/1.JPE.2.022004
- Wheeler NR, Bruckman LS, Ma J, Wang E, Wang CK, Chou I, Sun J, French RH (2013) Statistical and domain analytics for informed study protocols. In: 2013 IEEE Energytech, pp. 1–7. https://doi.org/10.1109/EnergyTech.2013.6645354
- 44. Wheeler NR, Gok A, Peshek TJ, Bruckman LS, Goel N, Zabiyaka D, Fagerholm CL, Dang T, Alcantara C, Terry ML, French RH (2015) A data science approach to understanding photovoltaic module degradation. In: Dhere NG, Wohlgemuth JH, Jones-Albertus R (eds) Reliability of photovoltaic cells, modules, components, and systems VIII, vol 9563. International Society for Optics and Photonics, Bellingham, p 95630. https://doi.org/10.1117/12.22092 04
- Bruckman LS, Wheeler NR, Ma J, Wang E, Wang CK, Chou I, Sun J, French RH (2013) Statistical and domain analytics applied to PV module lifetime and degradation science. IEEE Access 1:384–403. https://doi.org/10.1109/ACCESS.2013.2267611
- Q-Lab (2019) A choice of lamps for the QUV accelerated weathering tester, vol. LU-8160. https://www.q-lab.com/products/quv-weathering-tester/quv



- Murray MP, Bruckman LS, French RH (2012) Photodegradation in a stress and response framework: poly(methyl methacrylate) for solar mirrors and lens. J Photonics Energy 2(1):022004. https:// doi.org/10.1117/1.JPE.2.022004
- Committee AE (2020) ASTM E313: Standard practice for calculating yellowness and whiteness indices from instrumentally measured color coordinates. https://doi.org/10.1520/E0313-20
- Committee AD (2021) ASTM D1003: standard test method for haze and luminous transmittance of transparent plastics. https:// doi.org/10.1520/D1003-21
- French RH, Tran HV (2009) Immersion lithography: photomask and wafer-level materials. Annu Rev Mater Res 39(1):93–126. https://doi.org/10.1146/annurev-matsci-082908-145350
- Murray MP, Bruckman LS, French RH (2012) Durability of materials in a stress-response framework: acrylic materials for photovoltaic systems. In: MRS online proceedings library archive, vol. 1391. https://doi.org/10.1557/opl.2012.1241
- Kronemeijer AJ, Pecunia V, Venkateshvaran D, Nikolka M, Sadhanala A, Moriarty J, Szumilo M, Sirringhaus H (2014) Two-dimensional carrier distribution in top-gate polymer field-effect transistors: correlation between width of density of localized states and urbach energy. Adv Mater 26(5):728–733. https://doi.org/10.1002/adma.201303060
- (1991) The electronic density of states. In: Street RA (Ed.) Hydrogenated amorphous silicon. Cambridge solid state science series, pp. 62–94. Cambridge University Press, Cambridge. https://doi.org/10.1017/CBO9780511525247.004
- Yang MK, French RH, Tokarsky EW (2008) Optical properties of Teflon<sup>®</sup> AF amorphous fluoropolymers. J Micro/Nanolithogr MEMS MOEMS 7(3):033010. https://doi.org/10.1117/1.2965541
- Bahgat AA, El-Samanoudy MM, Sabry AI (1999) Optical and electrical properties of binary WO<sub>3</sub>-Pb<sub>3</sub>O<sub>4</sub> glasses. J Phys Chem Solids 60(12):1921–1931. https://doi.org/10.1016/S0022-3697(99)00211-5
- 56. Huang W-H, Wheeler N, Klinke A, Xu Y, Du W, Verma AK, Gok A, Gordon D, Wang Y, Liu J, Curran A, Fada J, Ma X, Braid J, Carter J, Bruckman L, French R (2018) netSEM: network structural equation modeling. The comprehensive R archive network
- Dirac PAM (1939) A new notation for quantum mechanics. In: Mathematical proceedings of the Cambridge philosophical society, vol. 35(3), pp., 416–418. https://doi.org/10.1017/S030500410 0021162
- 58. Martin JW, Dickens B, Waksman D, Bentz DP, Byrd WE, Embree E, Roberts WE (1987) Thermal degradation of poly(methyl methacrylate) at 50°C to 125°C. J Appl Polym Sci 34(1):377–393. https://doi.org/10.1002/app.1987.070340130
- 59. Shlyapintokh VY, Gol'Denberg VI (1974) Effect of photostabilizers on the rate of photodegradation of polymethylmethacrylate.

- Eur Polym J 10(8):679–684. https://doi.org/10.1016/0014-3057(74)90179-7
- Bowden MJ, Chandross EA, Kaminow IP (1974) Mechanism of refractive index increase in photosensitized poly(methyl methacrylate). Polym Eng Sci 14(7):494

  497. https://doi.org/10.1002/ pen.760140706
- 61. Franois-Heude A, Richaud E, Desnoux E, Colin X (2014) Influence of temperature, UV-light wavelength and intensity on polypropylene photothermal oxidation. Polym Degrad Stab 100:10–20. https://doi.org/10.1016/j.polymdegradstab.2013.12.038
- Gordon DA, Zhan Z, Bruckman LS (2019) Characterizing the weathering induced degradation of poly(ethylene-terephthalate) using parafac modeling of fluorescence spectra. Polym Degrad Stab 161:85–94. https://doi.org/10.1016/j.polymdegradstab.2019. 01.006
- Rashidian M, Dorranian D (2014) Low-intensity UV effects on optical constants of PMMA film. J Theor Appl Phys 8(2):121. https://doi.org/10.1007/s40094-014-0121-0
- Johnston PK, Doyle E, Orzel RA (1988) Acrylics: a literature review of thermal decomposition products and toxicity. J Am Coll Toxicol 7(2):139–200. https://doi.org/10.3109/109158188090145 19
- Babo S, Ferreira JL, Ramos AM, Micheluz A, Pamplona M, Casimiro MH, Ferreira LM, Melo MJ (2020) Characterization and long-term stability of historical PMMA: impact of additives and acrylic sheet industrial production processes. Polymers 12(1010):2198. https://doi.org/10.3390/polym12102198
- Ishida T, Kitagaki R, Hagihara H, Elakneswaran Y (2021) Role of moisture in photo-ageing -macromolecular architecture evolution of acrylic-urethane network. Polym Test 96:107123. https://doi. org/10.1016/j.polymertesting.2021.107123

Springer Nature or its licensor (e.g. a society or other partner) holds exclusive rights to this article under a publishing agreement with the author(s) or other rightsholder(s); author self-archiving of the accepted manuscript version of this article is solely governed by the terms of such publishing agreement and applicable law.

# **Authors and Affiliations**

Hein Htet Aung<sup>1,2</sup> · Donghui Li<sup>1,3</sup> · Jiqi Liu<sup>1</sup> · Chiara Barretta<sup>4</sup> · Yiyang Sheng<sup>5</sup> · Yea Jin Jo<sup>1</sup> · Jayvic C. Jimenez<sup>6,7</sup> · Erika I. Barcelos<sup>1,7</sup> · Gernot Oreski<sup>4</sup> · Roger H. French<sup>1,7,8,9</sup> · Laura S. Bruckman<sup>1,2</sup>

□ Laura S. Bruckman lsh41@case.edu

Hein Htet Aung hein.htetaung@case.edu

Donghui Li donghui.li@pnnl.gov Jiqi Liu jxl1763@case.edu

Chiara Barretta chiara.barretta@pccl.at

Yiyang Sheng ys811@georgetown.edu



Yea Jin Jo yeajin.jo@case.edu

Jayvic C. Jimenez jimenez45@llnl.gov

Erika I. Barcelos erika.barcelos@case.edu

Gernot Oreski gernot.oreski@pccl.at

Roger H. French roger.french@case.edu

- Department of Materials Science and Engineering, Case Western Reserve University, Cleveland, OH 44106, USA
- <sup>2</sup> Center for Materials Data Science for Reliability and Degradation: MDS-RELY, Case Western Reserve University, Cleveland, OH 44106, USA
- <sup>3</sup> Pacific Northwest National Laboratory, Richland, WA 99354, USA

- Polymer Competence Center Leoben GmbH, Roseggerstrasse 12, Leoben 8700, Austria
- Department of Mathematics, Applied Mathematics and Statistics, Case Western Reserve University, Cleveland, OH 44106, USA
- <sup>6</sup> Lawrence Livermore National Laboratory, Livermore, CA 94550, USA
- Materials Data Science for Stockpile Stewardship: Center of Excellence, Case Western Reserve University, Cleveland, OH 44106, USA
- Department of Computer and Data Sciences, Case Western Reserve University, Cleveland, OH 44106, USA
- Department of Macromolecular Science and Engineering, Case Western Reserve University, Cleveland, OH 44106, USA

